haematologica
Journal of The Ferrata Storti Foundation

Exploiting MYC-induced PARPness to target genomic instability in multiple myeloma

by Daniele Caracciolo, Francesca Scionti, Giada Juli, Emanuela Altomare, Gaetanina Golino, Katia Todoerti, Katia Grillone, Caterina Riillo, Mariamena Arbitrio, Michelangelo Iannone, Eugenio Morelli, Nicola Amodio, Maria Teresa Di Martino, Marco Rossi, Antonino Neri, Pierosandro Tagliaferri, and Pierfrancesco Tassone

Haematologica 2020 [Epub ahead of print]

Citation: Daniele Caracciolo, Francesca Scionti, Giada Juli, Emanuela Altomare, Gaetanina Golino, Katia Todoerti, Katia Grillone, Caterina Riillo, Mariamena Arbitrio, Michelangelo Iannone, Eugenio Morelli, Nicola Amodio, Maria Teresa Di Martino, Marco Rossi, Antonino Neri, Pierosandro Tagliaferri, and Pierfrancesco Tassone. Exploiting MYC-induced PARPness to target genomic instability in multiple myeloma.
Haematologica. 2020; 105:xxx
doi:10.3324/haematol.2019.240713

Exploiting MYC-induced PARPness to target genomic instability in multiple myeloma

Daniele Caracciolo[1], Francesca Scionti[1], Giada Juli[1], Emanuela Altomare[1], Gaetanina Golino[1], Katia Todoerti[2], Katia Grillone[1], Caterina Riillo[1], Mariamena Arbitrio[3], Michelangelo Iannone[3], Eugenio Morelli[4], Nicola Amodio[1], Maria Teresa Di Martino[1], Marco Rossi[1], Antonino Neri[2], Pierosandro Tagliaferri[1], and Pierfrancesco Tassone[1,5]

[1] Department of Experimental and Clinical Medicine, Magna Græcia University, Campus Salvatore Venuta, Catanzaro, Italy; [2] Department of Oncology and Hemato-oncology, University of Milan, and Hematology, Fondazione Cà Granda IRCCS Policlinico, Milan, Italy; [3]IRIB-CNR, Catanzaro, Italy; [4] Jerome Lipper Multiple Myeloma Center, Department of Medical Oncology, Dana-Farber Cancer Institute, Boston, MA; [5]Sbarro Institute for Cancer Research and Molecular Medicine, Center for Biotechnology, College of Science and Technology, Temple University, Philadelphia, PA;

Running title: PARP1 addiction in multiple myeloma

Acknowledgements: This work has been supported by the Italian Association for Cancer Research (AIRC) with "Special Program for Molecular Clinical Oncology–5 per mille", 2010/15 and its Extension Program" No. 9980, 2016/18 (PI: PT); and also by "Innovative Immunotherapeutic Treatments of Human Cancer" Multi Unit Regional No. 16695 (cofinanced by AIRC and the CARICAL foundation), 2015/18 (PI: PT). We thank Dr. Ivana Criniti for her study coordination support and editorial assistance.

[*]**Corresponding author**: Pierfrancesco Tassone, Department of Experimental and Clinical Medicine, Magna Græcia University, Campus Salvatore Venuta, Catanzaro, Italy; e-mail: tassone@unicz.it.

Abstract

Multiple Myeloma (MM) is a hematologic malignancy strongly characterized by genomic instability, which promotes disease progression and drug resistance. Since we previously demonstrated that LIG3-dependent repair is involved in the genomic instability, drug resistance and survival of MM cells, we here investigated the biological relevance of PARP1, a driver component of Alternative-Non Homologous End Joining (Alt-NHEJ) pathway, in MM. We found a significant correlation between higher PARP1 mRNA expression and poor prognosis of MM patients. PARP1 knockdown or its pharmacological inhibition by Olaparib impaired MM cells viability *in vitro* and was effective against *in vivo* xenografts of human MM. Anti-proliferative effects induced by PARP1-inhibition were correlated to increase of DNA double-strand breaks, activation of DNA Damage Response (DDR) and finally apoptosis. Importantly, by comparing a gene expression signature of PARP inhibitors (PARPi) sensitivity to our plasma cell dyscrasia (PC) gene expression profiling (GEP), we identified a subset of MM patients which could benefit from PARP inhibitors. In particular, Gene Set Enrichment Analysis (GSEA) suggested that high MYC expression correlates to PARPi sensitivity in MM. Indeed, we identified MYC as promoter of PARP1-mediated repair in MM and, consistently, we demonstrate that cytotoxic effects induced by PARP inhibition are mostly detectable on MYC-proficient MM cells.

Taken together, our findings indicate that MYC-driven MM cells are addicted to PARP1 Alt-NHEJ repair, which represents therefore a druggable target in this still incurable disease.

Introduction

Genomic instability represents a key hallmark of cancer since it progressively promotes the acquisition of features that lead to tumorigenesis. Indeed, almost all cancers are characterized by the tendency to accumulate genetic aberrations, such as gene copy-number variations (CNVs), translocations and mutations, which finally confer growth and survival advantage (1).

Genomic instability is strongly fostered by alteration of DNA repair pathways, which compromises "genomic guardian" mechanisms involved in prevention of neoplastic transformation. At the same time, DDR machinery represents a specific tumor "Acheel heel", since it could be therapeutically exploited by designing anticancer strategies targeting cancer DNA repair vulnerabilities with a synthetic lethality approach (2). The discovery that Homologous Recombination (HR) deficient tumors cells are specifically sensitive to inhibition of poly(ADP-ribose) polymerase 1 (PARP1) (3-5) provides an example of how to therapeutically exploit these vulnerabilities and led to the rapid development of several other DDR inhibitors such as ATM, ATR, CHK1 and CHK2, DNA-PK and WEE1 inhibitors (6). However, it remains unclear why a substantial number of patients who lack HR mutations still benefit from PARP inhibitor (7), a condition defined as "PARPness"(8).

Double strand breaks (DSBs) DNA lesions are mainly repaired by Classical Non-Homologous End Joining (C-NHEJ) (9) and HR (10). Recently, a third DSB repair pathway named Alternative-NHEJ (Alt-NHEJ) (11) has been demonstrated to function as error prone back-up pathway when the two major mechanisms are defective, contributing to the pathogenesis of several tumors (12-15). Multiple myeloma (MM) is a hematologic malignancy characterized by the growth of malignant plasma cells harboring numerous karyotypic aberrations (16). Indeed, the presence of specific cytogenetic abnormalities defines MM patients' subgroups with different prognosis requiring risk-adapted treatment. Although new therapeutics have prolonged survival of MM patients, cure for this disease is still an unmet need, and the identification of novel and actionable molecular drivers might provide innovative therapeutic approaches. It is known that genomic instability is a hallmark of MM but, to date, specific Achille's heels have not been identified.

PARP1 is the best-characterized member of the PARP family and play a crucial role in Alt-NHEJ pathway (17, 18). Indeed, it senses DNA damage via its DNA binding domain (19),

subsequently synthesizes Poly (ADP-ribose) (PAR) polymers which are added to itself and other acceptor proteins, thus recruiting other DNA repair proteins, including LIG3.
We have provided evidence that up-regulation of LIG3-mediated DNA repair plays a pivotal role in genomic instability and survival of MM cells (20). Starting from these data, we here report that PARP1 is crucial for survival of MYC-addicted MM cells, and we provide the rational framework for the use of PARP inhibitors as therapeutic strategy in this still incurable disease.

Methods

For a more detailed description of the methods used, see supplementary methods (available on the online version of paper).

Cell lines and primary tumor specimens

Cell lines were obtained from the ATCC or kindly provided by sources indicated in Supplementary Methods.

Analysis of cell viability and apoptosis

Cell viability was analyzed by Cell Titer-Glo assay (CTG; Promega, Madison, WI, USA); apoptosis was evaluated by flow cytometric (Attune NxT Flow cytometer, Thermo Fisher Scientific) analysis following Annexin V-7AAD staining (BD Pharmingen).

Cell cycle analysis

Analysis of cell cycle was performed by Propidium Iodide flow cytometry assay (BD Pharmingen), according to manufacturer's instructions. Flow cytometry analysis was performed by Attune NxT Flow cytometer (Thermo Fisher Scientific).

Western blot analysis

Whole cell protein extracts were prepared from MM cells and from Peripheral Blood Mononuclear Cells (PBMCs) in NP40 Cell Lysis Buffer (Novex®) containing a cocktail of protease inhibitors (Sigma, Steinheim, Germany). Cell lysates were loaded and PAGE separated. Proteins were transferred by Trans-Blot® TurboTM Transfer Starter System for 7 min. After protein transfer, the membranes were blotted with antibodies listed in

the Supplementary table and visualized with C-DiGit® Blot Scanner (LI-COR) by using the ECL Western Blotting Detection Reagents (Thermo Fisher Scientific, IL). Image capture was carried out using image studio® (LI-COR, version 5.0) software.

Immunofluorescence

Cells were harvested, centrifuged onto glass slides (Cytospin 4, Thermo Scientific), and fixed in 4% paraformaldehyde in PBS, pH 7.4, for 12 min at 22°C, followed by three 5-min washes in PBS. Cells were permeabilized (0.1% Triton X-100 in PBS, 15-min), washed in PBS (3×, 5 min each), and incubated 1 h at 22°C with blocking buffer (1.5% BSA in PBS). They were reacted >12 h at 4°C with primary antibodies listed in the Supplementary table, washed in PBS (3×, 5 min each), and incubated 1 h at 22°C in the dark, with appropriate secondary antibodies. Cells were washed 3× in PBS and mounted under coverslips with Vectashield with DAPI (Vector Laboratories). Images were acquired with an SP2 Leica Zeiss confocal laser-scanning microscope with a 63× oil objective.

Animals and in vivo models of human MM

Male CB-17 severe combined immunodeficient (SCID) mice (6- to 8-weeks old; Harlan Laboratories, Inc., Indianapolis) were housed and monitored in our Animal Research Facility. Experimental procedures and protocols had been approved by the Magna Graecia University IRB and conducted according to protocols approved by the National Directorate of Veterinary Services (Italy). Mice were subcutaneous inoculated with $5x10^6$ H929 or ABZB cells and treatment started when palpable tumors became detectable (100–200 mm^3). Animals were daily treated with Olaparib (Selleckchem) (100mg/Kg) or vehicle [10%v/v DMSO in 10%w/v Kleptose (HP-β-CD) in purified de-ionised water] via oral gavage. Tumor sizes were measured as described (21), and the investigator was blinded to group allocation.

Statistical Analysis

Each experiment was performed at least 3 times and values are reported as means ±SD. Comparisons between groups were made with student's t-test, while statistical significance of differences among multiple groups was determined by GraphPad software (www.graphpad.com). Graphs were obtained using Graphpad Prism version 6.0. p-value of less than 0.05 was accepted as statistically significant.

Results

High PARP1 expression occurs in MM and predicts for poor prognosis

To understand the role of PARP1 in the pathophysiology of MM, the prognostic relevance of mRNA expression was investigated. Indeed, analysis of public MM datasets revealed that higher PARP1 mRNA expression was significantly correlated with shorter Overall Survival (OS) and Event Free Survival (EFS) (Figure 1A), thus highlighting its pivotal contribute to disease pathogenesis. Indeed, PARP1 mRNA expression increased during disease progression and in high-risk MM subgroups harboring t(4;14) and t(14;16) translocations (TC4 and TC5) (Figure 1B, Supplementary Figure 1A)(22). Of note, no significant influence of copy number on PARP1 expression gene was found (Supplementary Figure 1B), thus suggesting that high expression of PARP1 in MM patients could be derived from deregulation of transcriptional or post-transcriptional mechanisms that normally regulate PARP1 expression. Notably PARP1 mRNA was the most expressed among other PARP family members. Furthermore, mRNA expression of other PARPs did not retain any prognostic relevance, except for PARP2 (Supplementary Figure 1C-D).

Moreover analysis of GSE9782 dataset revealed that higher levels of PARP1 mRNA predicted poor OS and Progression Free Survival (PFS) for patient who received Bortezomib-based therapy (Figure 1C). Overall, these findings strongly suggest involvement of PARP1 in the genomic instability of MM, which promotes disease progression and drug resistance.

PARP1 is a therapeutic target in MM

Based on clinical findings, which suggested a relevant role of PARP1 in MM pathogenesis, protein levels were analyzed in a panel of MM cell lines, primary cells from MM patients and healthy donors (HDs) PBMCs. As shown in Figure 2A, up-regulation of PARP1 protein expression with a nuclear distribution in MM cells as compared to HD PBMCs, was observed. In particular PARP1 protein was undetectable only in 1 of 4 primary MM cells evaluated and in U266 cell line.

To investigate its biological relevance in MM cells, knockdown experiments were performed to evaluate whether PARP1 was required for MM cell viability. Importantly, PARP1 down-regulation significantly reduced viability and increased apoptosis of MM cell line (Figure 2B, Supplementary Fig. 2A).

Then, the effects on MM cells survival induced by clinical available PARP 1/2 inhibitor Olaparib were investigated. Importantly, MM cells were highly sensitive to Olaparib with an IC50<10 uM observed in 7 of 8 tested cell lines (Figure 2C). In particular, IC50 was 0,5 uM in NCI-H929, KMS-12BM, KMS26 and INA-6, as in the highly sensitive BRCA2-defective CAPAN1 cells (Pancreatic adenocarcinoma cell line), which were used as positive control cell line in this experiment (23). Moreover, Olaparib induced an increase of apoptotic cell death and a reduction of clonogenic growth in a dose dependent manner (Supplementary Figures 2 B-C). Importantly, Olaparib impaired the viability of primary MM plasma cells co-cultured with stromal cells (Figure 2C), thus overcoming protective role of bone marrow (BM) microenvironment. To confirm the translational relevance of our in vitro findings, *in vivo* anti-MM activity of Olaparib was evaluated resulting in a significant tumor-growth inhibition (Figure 2E).

Finally, the basal expression of the other Olaparib target PARP2 was evaluated. Notably, a very lower protein expression as compared to PARP1 was found (Supplementary Figure 2D), thus suggesting a minor role of PARP2 in driving Olaparib activity in MM cell lines.

Overall, these findings greatly suggest PARP1 as promising therapeutic target in MM.

PARP1 inhibition triggers DDR response in MM cells

Since PARP1 plays a critical role in DSBs repair, the effect of PARP1 inhibition on DDR was investigated. Importantly, Olaparib treatment induced a relevant increase of unrepaired DNA damage, along with a significant activation of DDR and apoptosis signaling, as demonstrated by increased phosphorylation of ATM, ATR, CHK1, CHK2, H2AX, occurring together with PARP1 and caspase-3 cleavage (Figure 3A). Similar results were also obtained after PARP1 knockdown in MM cell lines or after Olaparib treatment in primary MM cells (Supplementary Figures 3A-B).

Cell cycle analysis revealed also G2-arrest after Olaparib treatment (Figure 3B), which was abrogated by caffeine (24) (Supplementary Figure 3C), thus suggesting that checkpoint activation induced by Olaparib treatment depend on ATM/ATR signaling.

To investigate molecular mechanisms underpinning the increase of DNA DSBs observed after Olaparib treatment, functional experiments were performed. To this aim, the activity of Alt-NHEJ repair was evaluated given the pivotal role exerted by PARP1 in this DNA repair pathway. Indeed, Alt-NHEJ repair was clearly reduced in MM cells treated with Olaparib as compared to vehicle alone (Figure 3C, Supplementary Figure 3D).

To investigate if PARP trapping onto damaged DNA is responsible of cytotoxic activity of PARPi, R8226 cell lysates were fractionated into nuclear-soluble and chromatin-bound fractions. Notably, although PARylation were reduced by treatment, Olaparib alone not significantly increased PARP1 chromatin binding as compared to nuclear-soluble fraction (Figure 3D), suggesting that Olaparib effects in MM are correlated to inhibition of DSB repair rather than to PARP-trapping activity.

MYC drives sensitivity to Parp-inhibition

To identify predictive biomarkers for PARPi in MM, a published PARPi response gene expression signature (25) was evaluated in a proprietary plasma cell (PC) dyscrasias dataset, previously analyzed by global gene expression profiling (GEP) using microarray technology (26). Particularly, a great part of secondary plasmacell leukemia (sPCL) samples and human myeloma cell lines (HMCLs) showed PARPi-positive expression pattern, MM samples showed heterogeneous expression levels, whereas primary plasmacell leukemia (pPCL) cases mostly evidenced an opposite expression trend. Notably, among MM-TC classes, half MM-TC2 cases were grouped together with majority of sPCL and all HMCLs PARPi-positive clusters (Figure 4A). Therefore, in order to identify concordantly modulated sets of genes that were potentially associated to PARPi signature in MM, PARPi-positive and PARPi-negative MM-TC2 cases were compared by GSEA analysis (27). Interestingly, groups of genes regulated by MYC and involved in DNA repair resulted among the most significantly up-regulated in PARPi-positive versus PARPi-negative cases (Figure 4B, Supplementary Figure 4A). Similar results were also obtained comparing PARPi-positive and PARPi-negative PCL cases. Accordingly, MYC transcript reached the highest median expression levels in sPCL and HMCLs across PC dyscrasia groups and in MM-TC2 class (Supplementary Figure 4B).

To validate bioinformatics results, MYC protein basal levels were evaluated in Olaparib tested MM cell lines. Notably, Olaparib insensitive U266 cells did not express MYC protein (Supplementary Figure 4C)(28). Next, Olaparib was tested on P936 B cell-like lymphoma cells, a cellular models wherein MYC levels could be turned on/off by adding Doxycycline. Notably, Olaparib treatment effectively induced cell death only at Myc-*on* conditions. Conversely, as formal proof of our hypothesis, overexpression of MYC in U266 cells (MYC-OE) restored cell death upon PARP1 knockdown or PARP1 inhibitor treatment (Figure 4C, Supplementary Figure 4D). Moreover, the lack of correlation between PARP

inhibitor sensitivity and the evidence of HR deficiency (as evaluated by RAD51 protein levels), or the presence of MM characteristic cytogenetic abnormalities (13q deletion, 1q gain, hyperdyploidy) or somatic mutations (BRAF, NRAS, KRAS, DIS3) (Supplementary Figure 4E), further support the hypothesis that PARP-inhibition triggers MYC-dependent synthetic lethality in MM.

Bortezomib resistant cells are highly sensitive to PARP inhibition

Based on clinical data, which suggest a potential role in Bortezomib resistance (Figure 1C), the effects of PARP1-inhibition in this context was also investigated. Notably, AMO1 bortezomib resistant (ABZB) cells showed higher Alt-NHEJ repair and CNVs as compared to their sensitive counterpart AMO1 cells (Figure 5A), thus suggesting an association between genomic instability increase and Bortezomib resistance acquirement. Interestingly, enforced expression of PARP1 on AMO1 cells significantly antagonized the effect induced by Bortezomib on cell viability (Figure 5B).

Importantly, Olaparib showed significant growth inhibitory activity against ABZB cells *in vitro* and *in vivo* (Figure 5C, Supplementary Figures 5A-B).

Since higher protein levels of PARP1 and MYC were observed in ABZB cells as compared to AMO1 (Figure 5D), a potential role of MYC in PARP1 transcription was next investigated.

Notably, analysis of multiple myeloma patients' dataset (GSE24080), showed a significant positive correlation between PARP1 and MYC expression (Supplementary Figure 5C). Indeed, a bioinformatic screening (cistrome.org) showed a significant enrichment of MYC binding consensus sequences to PARP1 promoter (Supplementary Figure 5D), which was next validated by Chip analysis (Figure 5E). Therefore, siRNA-mediated knockdown of MYC induced a down-regulation of PARP1 protein and a decrease of promoter activity (Figure 5E) indicating that MYC binds to PARP1 promoter modeling its transcription.

Discussion

DDR presents an attractive area of investigation for the opportunity to selectively kill cancer cells addicted to compensatory DNA repair pathways by synthetic lethality (29). There is experimental evidence that Alt-NHEJ is an error-prone DNA repair pathway (30-35) and master driver of genomic instability in cancer (36).

In this study, we investigated the involvement of PARP1, a pivotal component of error-

prone Alt-NHEJ repair, in the pathogenesis of MM genomic instability (37).

Indeed, Alt-NHEJ repair pathway is involved in important processes of B-lineage differentiation such as VD-J recombination and class switch recombination (CSR) (38), critical steps where errors in the rearrangement of the germ-line DNA could generate translocation of proto-oncogenes, such as MYC (39), into the immunoglobulin (Ig) loci, thus potentially contributing to myelomagenesis.

Consistently, we found that high PARP1 mRNA expression is significantly correlated to poor EFS and OS in MM patients, and increases during disease progression and in high-risk cases. Moreover, PARP1 mRNA is the most expressed among PARP family members, thus suggesting a critical role of PARP1 in MM pathogenesis. In fact, we found that PARP1 knockdown induces MM cell death.

In the aim of translating these findings into the design of a new therapeutic strategy, we provide evidence that Olaparib, an available PARPi, induces anti-MM activity at clinical doses (40), including against Bortezomib-resistant MM cells. Growth inhibitory effects induced by Olaparib, were correlated to Alt-NHEJ inhibition (41) which led to increase of unrepaired DNA damage and apoptotic cell death.

To investigate mechanisms leading to PARPi sensitivity in MM, we used a PARP inhibition sensitivity gene expression signature (25). Interestingly our analysis highlighted a pivotal role of MYC, a driver transcription factor hyper-activated in majority of MM patients (42, 43). Indeed, the signature was enriched in TC2 MM patients and secondary PCL subgroups, which display the highest MYC expression (44). Consistently, we show here that PARP inhibition induces cytotoxic effects against MM, which mostly occur on MYC proficient cells.

Our findings are consistent with recent reports showing that MYC-dependent Burkitt lymphoma (45) and neuroblastoma (46) are sensitive to PARPi. Indeed, MYC drives genomic instability by deregulation of DDR, thus increasing cancer cells dependency from low-fidelity DNA repair pathways (47-49). Moreover, MYC is a strong inducer of replication stress, which requires DDR activation to repair DNA damage and to sustain cell survival (50, 51).

On these findings, we hypothesize that MYC-driven MM cells switch their DNA repair machinery to error-prone PARP-mediated Alt-NHEJ. This event allows to overcome DNA damage overload from oncogenic stress, promoting cell survival and, at the same time, the acquisition of new genetic changes leading to disease progression (Figure 6). Indeed, it

could be hypothesized that MYC induces Alt-NHEJ repair to balance HR down-regulation induced by Bortezomib (52, 53), contributing to development of drug resistance and, at the same time, making MM cells more dependent from PARP1-mediated DNA repair to survive. Consistently, we also report here that Bortezomib-resistant MM cells are extremely sensitive to PARP-inhibition. This finding is of translational relevance, since it could support the design of a maintenance therapy with PARP-inhibitors as strategy to prevent disease progression and drug resistance acquirement.

In conclusion, our study demonstrates addiction of MYC-driven MM cells to PARP1, which could be exploited as a new opportunity for synthetic lethality in the clinical scenario of precision oncology. Moreover our findings highlight the role of MYC as driver of PARP1-mediated repair, identifying a novel mechanism of genome stability and survival regulation and a potential biomarker of PARPness in this still incurable disease.

Supplementary information

Supplementary information is available at Haematologica website.

Conflict of Interest Disclosures: The authors declare no competing financial interests.

References

1. Hanahan D, Weinberg RA. Hallmarks of cancer: the next generation. Cell. 2011;144(5):646-674.

2. Murata S, Zhang C, Finch N, et al. Predictors and Modulators of Synthetic Lethality: An Update on PARP Inhibitors and Personalized Medicine. Biomed Res Int. 2016;2016:2346585.

3. Kim G, Ison G, McKee AE, et al. FDA Approval Summary: Olaparib Monotherapy in Patients with Deleterious Germline BRCA-Mutated Advanced Ovarian Cancer Treated with Three or More Lines of Chemotherapy. Clin Cancer Res. 2015;21(19):4257-4261.

4. Balasubramaniam S, Beaver JA, Horton S, et al. FDA Approval Summary: Rucaparib for the Treatment of Patients with Deleterious BRCA Mutation-Associated Advanced Ovarian Cancer. Clin Cancer Res. 2017;23(23):7165-7170.

5. [No authors listed]. Olaparib for Metastatic Breast Cancer in Patients with a Germline BRCA Mutation. N Engl J Med. 2017;377(17):1700.

6. Ashworth A, Lord CJ. Synthetic lethal therapies for cancer: what's next after PARP inhibitors? Nat Rev Clin Oncol. 2018;15(9):564-576.

7. Pilie PG, Gay CM, Byers LA, O'Connor MJ, Yap TA. PARP Inhibitors: Extending Benefit Beyond BRCA-Mutant Cancers. Clin Cancer Res. 2019;25(13):3759-3771.

8. Pilie PG, Tang C, Mills GB, Yap TA. State-of-the-art strategies for targeting the DNA damage response in cancer. Nat Rev Clin Oncol. 2019;16(2):81-104.

9. Pannunzio NR, Watanabe G, Lieber MR. Nonhomologous DNA end-joining for repair of DNA double-strand breaks. J Biol Chem. 2018;293(27):10512-10523.

10. San Filippo J, Sung P, Klein H. Mechanism of eukaryotic homologous recombination. Annu Rev Biochem. 2008;77:229-257.

11. Chang HHY, Pannunzio NR, Adachi N, Lieber MR. Non-homologous DNA end joining and alternative pathways to double-strand break repair. Nat Rev Mol Cell Biol. 2017;18(8):495-506.

12. Fan J, Li L, Small D, Rassool F. Cells expressing FLT3/ITD mutations exhibit elevated repair errors generated through alternative NHEJ pathways: implications for genomic instability and therapy. Blood. 2010;116(24):5298-5305.

13. Newman EA, Lu F, Bashllari D, et al. Alternative NHEJ Pathway Components Are Therapeutic Targets in High-Risk Neuroblastoma. Mol Cancer Res. 2015;13(3):470-482.

14. Tobin LA, Robert C, Nagaria P, et al. Targeting abnormal DNA repair in therapy-resistant breast cancers. Mol Cancer Res. 2012;10(1):96-107.

15. Ceccaldi R, Liu JC, Amunugama R, et al. Homologous-recombination-deficient tumours are dependent on Poltheta-mediated repair. Nature. 2015;518(7538):258-262.

16. Neri P, Bahlis NJ. Genomic instability in multiple myeloma: mechanisms and therapeutic implications. Expert Opin Biol Ther. 2013;13 Suppl 1:S69-82.

17. Krishnakumar R, Kraus WL. The PARP side of the nucleus: molecular actions, physiological outcomes, and clinical targets. Mol Cell. 2010;39(1):8-24.

18. Paddock MN, Bauman AT, Higdon R, et al. Competition between PARP-1 and Ku70 control the decision between high-fidelity and mutagenic DNA repair. DNA Repair (Amst). 2011;10(3):338-343.

19. Yang G, Liu C, Chen SH, et al. Super-resolution imaging identifies PARP1 and the Ku complex acting as DNA double-strand break sensors. Nucleic Acids Res. 2018;46(7):3446-3457.

20. Caracciolo D, Di Martino MT, Amodio N, et al. miR-22 suppresses DNA ligase III addiction in multiple myeloma. Leukemia. 2019;33(2):487-498.

21. Leone E, Morelli E, Di Martino MT, et al. Targeting miR-21 inhibits in vitro and in vivo multiple myeloma cell growth. Clin Cancer Res. 2013;19(8):2096-2106.

22. Zhan F, Huang Y, Colla S, et al. The molecular classification of multiple myeloma. Blood. 2006;108(6):2020-2028.

23. McCabe N, Lord CJ, Tutt AN, et al. BRCA2-deficient CAPAN-1 cells are extremely sensitive to the inhibition of Poly (ADP-Ribose) polymerase: an issue of potency. Cancer Biol Ther. 2005;4(9):934-936.

24. Sarkaria JN, Busby EC, Tibbetts RS, et al. Inhibition of ATM and ATR kinase activities by the radiosensitizing agent, caffeine. Cancer Res. 1999;59(17):4375-4382.

25. McGrail DJ, Lin CC, Garnett J, et al. Improved prediction of PARP inhibitor response and identification of synergizing agents through use of a novel gene expression signature generation algorithm. NPJ Syst Biol Appl. 2017;3:8.

26. Lionetti M, Barbieri M, Todoerti K, et al. Molecular spectrum of BRAF, NRAS and KRAS gene mutations in plasma cell dyscrasias: implication for MEK-ERK pathway activation. Oncotarget. 2015;6(27):24205-24217.

27. Subramanian A, Tamayo P, Mootha VK, et al. Gene set enrichment analysis: a knowledge-based approach for interpreting genome-wide expression profiles. Proc Natl Acad Sci U S A. 2005;102(43):15545-15550.

28. Dib A, Gabrea A, Glebov OK, Bergsagel PL, Kuehl WM. Characterization of MYC translocations in multiple myeloma cell lines. J Natl Cancer Inst Monogr. 2008;(39):25-31.

29. Hartwell LH, Szankasi P, Roberts CJ, Murray AW, Friend SH. Integrating genetic approaches into the discovery of anticancer drugs. Science. 1997;278(5340):1064-1068.

30. Iliakis G, Murmann T, Soni A. Alternative end-joining repair pathways are the ultimate backup for abrogated classical non-homologous end-joining and homologous recombination repair: Implications for the formation of chromosome translocations. Mutat Res Genet Toxicol Environ Mutagen. 2015;793:166-175.

31. Arana ME, Seki M, Wood RD, Rogozin IB, Kunkel TA. Low-fidelity DNA synthesis by human DNA polymerase theta. Nucleic Acids Res. 2008;36(11):3847-3856.

32. Wood RD, Doublie S. DNA polymerase theta (POLQ), double-strand break repair, and cancer. DNA Repair (Amst). 2016;44:22-32.

33. Zhuang J, Jiang G, Willers H, Xia F. Exonuclease function of human Mre11 promotes deletional nonhomologous end joining. J Biol Chem. 2009;284(44):30565-30573.

34. Taylor RM, Whitehouse CJ, Caldecott KW. The DNA ligase III zinc finger stimulates binding to DNA secondary structure and promotes end joining. Nucleic Acids Res. 2000;28(18):3558-3563.

35. Simsek D, Brunet E, Wong SY, et al. DNA ligase III promotes alternative nonhomologous end-joining during chromosomal translocation formation. PLoS Genet. 2011;7(6):e1002080.

36. Caracciolo DM, M.; Tagliaferri, P.; Tassone,P. Alternative non-homologous end joining repair: a master regulator of genomic instability in cancer[Review]. Prec Cancer Med. 2019;2:8.

37. Morgan GJ, Walker BA, Davies FE. The genetic architecture of multiple myeloma. Nat Rev Cancer. 2012;12(5):335-348.

38. Boboila C, Jankovic M, Yan CT, et al. Alternative end-joining catalyzes robust IgH locus deletions and translocations in the combined absence of ligase 4 and Ku70. Proc Natl Acad Sci U S A. 2010;107(7):3034-3039.

39. Mikulasova A, Ashby C, Tytarenko RG, et al. Microhomology-mediated end joining drives complex rearrangements and over expression of MYC and PVT1 in multiple myeloma. Haematologica. 2019 June 20. [Epub ahead of Print]

40. Fong PC, Boss DS, Yap TA, et al. Inhibition of poly(ADP-ribose) polymerase in tumors from BRCA mutation carriers. N Engl J Med. 2009;361(2):123-134.

41. Howard SM, Yanez DA, Stark JM. DNA damage response factors from diverse pathways, including DNA crosslink repair, mediate alternative end joining. PLoS Genet. 2015;11(1):e1004943.

42. Chesi M, Robbiani DF, Sebag M, et al. AID-dependent activation of a MYC transgene induces multiple myeloma in a conditional mouse model of post-germinal center malignancies. Cancer Cell. 2008;13(2):167-180.

43. Kuehl WM, Bergsagel PL. MYC addiction: a potential therapeutic target in MM. Blood. 2012;120(12):2351-2352.

44. Weinhold N, Kirn D, Seckinger A, et al. Concomitant gain of 1q21 and MYC translocation define a poor prognostic subgroup of hyperdiploid multiple myeloma. Haematologica. 2016;101(3):e116-119.

45. Maifrede S, Martin K, Podszywalow-Bartnicka P, et al. IGH/MYC Translocation Associates with BRCA2 Deficiency and Synthetic Lethality to PARP1 Inhibitors. Mol Cancer Res. 2017;15(8):967-972.

46. Colicchia V, Petroni M, Guarguaglini G, et al. PARP inhibitors enhance replication stress and cause mitotic catastrophe in MYCN-dependent neuroblastoma. Oncogene. 2017;36(33):4682-4691.

47. Li Z, Owonikoko TK, Sun SY, et al. c-Myc suppression of DNA double-strand break repair. Neoplasia. 2012;14(12):1190-1202.

48. Muvarak N, Kelley S, Robert C, et al. c-MYC Generates Repair Errors via Increased Transcription of Alternative-NHEJ Factors, LIG3 and PARP1, in Tyrosine Kinase-Activated Leukemias. Mol Cancer Res. 2015;13(4):699-712.

49. Zhang W, Liu B, Wu W, et al. Targeting the MYCN-PARP-DNA Damage Response Pathway in Neuroendocrine Prostate Cancer. Clin Cancer Res. 2018;24(3):696-707.

50. Cottini F, Hideshima T, Suzuki R, et al. Synthetic Lethal Approaches Exploiting DNA Damage in Aggressive Myeloma. Cancer Discov. 2015;5(9):972-987.

51. Kotsantis P, Petermann E, Boulton SJ. Mechanisms of Oncogene-Induced Replication Stress: Jigsaw Falling into Place. Cancer Discov. 2018;8(5):537-555.

52. Neri P, Ren L, Gratton K, et al. Bortezomib-induced "BRCAness" sensitizes multiple myeloma cells to PARP inhibitors. Blood. 2011;118(24):6368-6379.

53. Pawlyn C, Loehr A, Ashby C, et al. Loss of heterozygosity as a marker of homologous repair deficiency in multiple myeloma: a role for PARP inhibition? Leukemia. 2018;32(7):1561-1566.

Legend to figures

Figure 1. **High PARP1 levels are associated with poor prognosis in MM patients**. **(A)** Data obtained interrogating GSE24080 dataset by PRECOG software (https://precog.stanford.edu/index.php). Prognostic relevance of PARP1 mRNA (NM_208644_at) expression, on OS and EFS of MM patients. **(B)** PARP1 mRNA expression analysis from proprietary datasets. *Left panel*: PARP1 levels in healthy donors as compared to MM and primary (p) and secondary (s) PCL cases. *Right panel*: PARP1 expression MM patients according to TC classification. **(C)** Analysis of GSE9782 dataset by using GenomicScape software (www.genomicscape.com). Prognostic relevance of PARP1 levels on OS and PFS of MM patients enrolled to Bortezomib therapy. *, P<0.05; **, P<0.01

Figure 2. **Addiction of MM cells to PARP1 (A)** *Left panel*: Immunoblot of PARP1 performed on PBMCs collected from healthy donors, MM cell lines and patients (Pts). GAPDH was used as a loading control. *Right panel*: Immunofluorescence analysis showing subcellular distribution of PARP1 in R8226 and patient (Pt#2) MM cells (magnification 20x): PARP1 (green); DAPI (blue) was used for nuclear staining. **(B)** Indicated cell lines were transfected with scramble control or PARP1-siRNA. *Top:* CTG assay was performed 4 days after transfection. *Bottom:* Immunoblot analysis of PARP1. GAPDH was used as a loading control. Analysis was performed 48h after transfection. **(C)** Indicated MM cells were treated with increasing dose of Olaparib. *Left panel*: CTG assay was performed 7 days from treatment. Results are expressed as percentage of vehicle treated cells. **(D)** Cell viability of CD138+ cells from 4 different MM patients co-cultured with HS-5 stromal cells and treated with Olaparib 5 uM or vehicle. The assay was performed 4 days after treatment. **(E)** *In vivo* growth of H929 subcutaneous xenograft daily treated with vehicle or Olaparib (100mg/Kg) via oral gavage. Averaged tumor volume of each group ± SD is shown.

Data are representative of at least three independent experiments. *P<0.05; **P<0.01.

Figure 3. Olaparib activates DDR in MM cells. **(A)** R8226 and H929 cells were treated with Olaparib. *Left panel*: Immunoblot analysis was performed 24 hours after treatment. *Right panel:* γ-H2AX foci evaluation by immunofluorescence. Representative images of unrepaired DSBs are shown. DAPI (blue) was used for nuclear staining. **(B)** Cell cycle

analysis performed 24h after treatment of H929 and R8226 cell with Olaparib (2,5 uM). **(C)** Alt-NHEJ repair was evaluated by EJ2-GFP assay on R8226 cells 48h after Olaparib (2,5 uM) treatment. **(D)** Western blot analysis of nuclear soluble and chromatin bound fractions prepared from R8226 cells. Cells were treated for 30 min with vehicle or Olaparib as indicated. Histone H3 and LAMIN A/C were used as positive markers for chromatin and nuclear soluble fractions, respectively.
Data are representative of at least three independent experiments. *P<0.05; **P<0.01.

F**igure 4**. **MYC drives sensitivity to Parp-inhibition (A)** Hierarchical agglomerative clustering of PC dyscrasias' samples on PARPi gene expression signature. Type of samples (N, MM, PPCL, SPCL, HMCL) and MM TC classes (TC1, TC2, TC3, TC4, TC5) are depicted in different colors. The color scale bar represents the relative gene expression changes normalized by the standard deviation. PPCL, SPCL and MM-TC2 significant clusters are highlighted: 16/24 pPCL, p-value=$4x10^{-4}$; 7/12 sPCL p-value=$8.4x10^{-3}$; 8/30 TC2, p-value=$6.5x10^{-3}$; 7/30 TC2, p-value=$9.4x10^{-3}$. **(B)** Enrichment plots of selected significant (nominal p-value < 0.05) gene sets by GSEA analysis on PARPi-positive versus PARPi-negative MM-TC2 cases. NES values are indicated. **(C)** *Left panel*: Cell viability analysis in P493-6 after 7 days of exposure to vehicle or Olaparib (5 uM), in presence (low Myc) or absence (high Myc) of doxycycline (500 ng/mL). *Right panel*: Cell viability analysis in U266 empty vector (EV) and U266 MYC+ after 7 days of exposure to vehicle or Olaparib (5 uM).
Data are representative of at least three independent experiments. *P<0.05; **P<0.01.

F**igure 5**. **Bortezomib resistant cells are highly sensitive to PARP inhibitors**
(A) *Left:* Alt-NHEJ repair was evaluated by EJ2-GFP assay on AMO1 and ABZB cells. *Right:* Affymetrix CytoScan HD Array analysis of CNVs, using genomic DNA from AMO1 and ABZB. **(B)** CTG Assay was performed on AMO1 transfected with PARP1 ORF or control ORF (EV) and then treated for 24h with increasing dose of Bortezomib. PARP1 overexpression was confirmed by western blot analysis. **(C)** *In vivo* growth of luciferase gene-marked Abzb xenografts daily treated with vehicle or Olaparib (100mg/Kg) via oral gavage. (c) *Left:* Averaged tumor volume of each group ± SD is shown. *P<0.05; **P<0.01. *Right:* PAR levels and Ki67 and HE expression were evaluated respectively by Western

Blot and IHC analysis (20x, 40x insets) from a representative ABZB xenograft per group. **(D)** *Left:* Immunoblot of PARP1 and MYC performed on AMO1 and ABZB. GAPDH was used as a loading control. *Right:* qPCR for PARP1 promoter performed after ChIP with MYC antibody in AMO1 and ABZB cells compared with negative (Ch22) and IgG controls. **(E)** *Left:* ABZB cells were transfected with siRNA-NC or MYC-siRNA. Immunoblot of PARP1 and MYC was performed 48h after transfection. *Right:* Promoter activity of transfected PARP1 and negative CTRL promoter constructs in ABZB cells co-transfected with either siRNA-NC or MYC-siRNA.

Data are representative of at least three independent experiments. *P<0.05; **P<0.01.

Figure 6. **Esplicative cartoon describing the addiction of MYC-driven MM cells to PARP1**

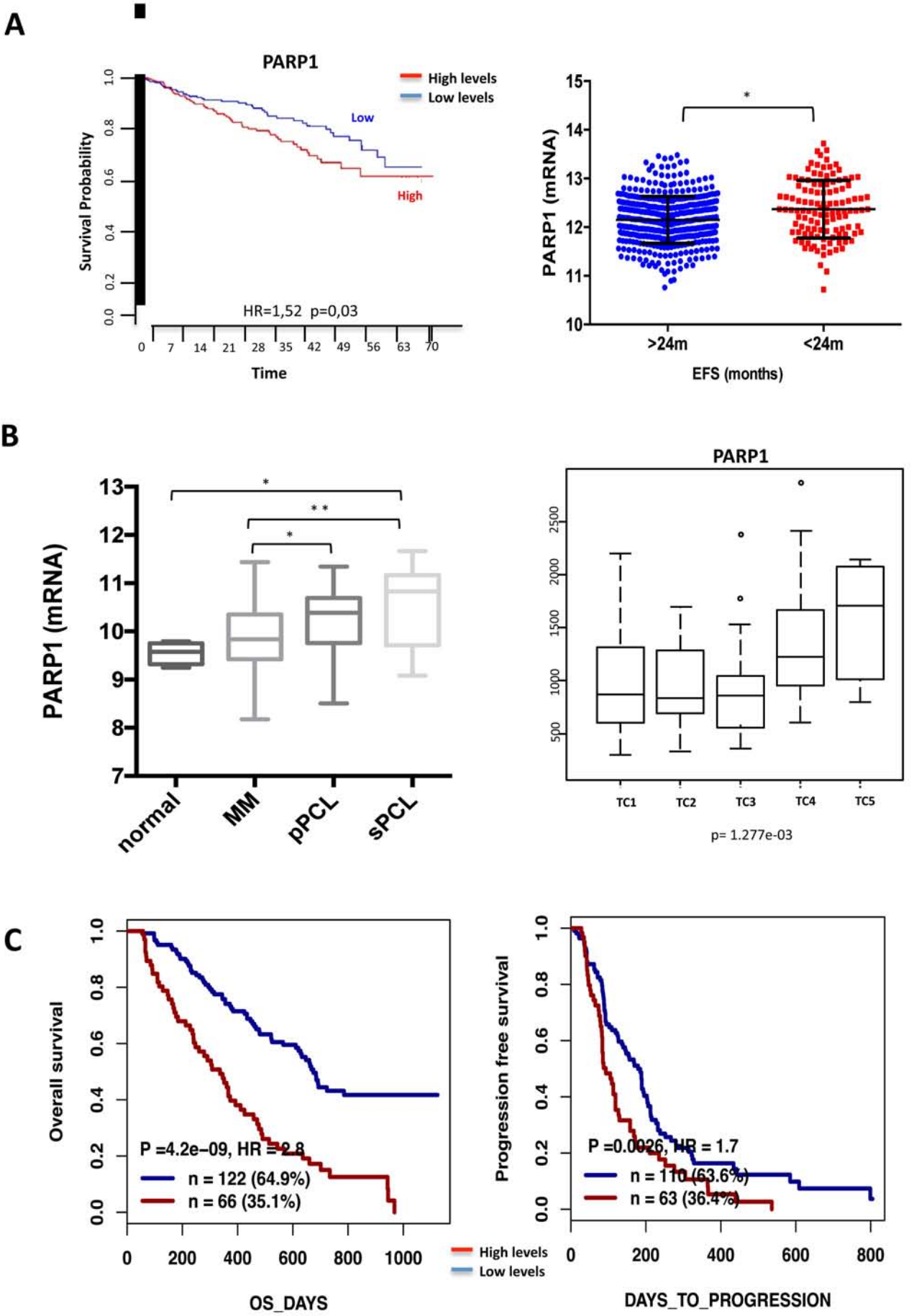
A
PARP1
High levels
Low levels
Low
High
Survival Probability
HR=1,52 p=0,03
Time
PARP1 (mRNA)
>24m
<24m
EFS (months)
B
PARP1 (mRNA)
normal
MM
pPCL
sPCL
PARP1
TC1
TC2
TC3
TC4
TC5
p= 1.277e-03
C
Overall survival
P =4.2e−09, HR = 2.8
n = 122 (64.9%)
n = 66 (35.1%)
OS_DAYS
Progression free survival
P =0.0026, HR = 1.7
n = 110 (63.6%)
n = 63 (36.4%)
DAYS_TO_PROGRESSION
High levels
Low levels

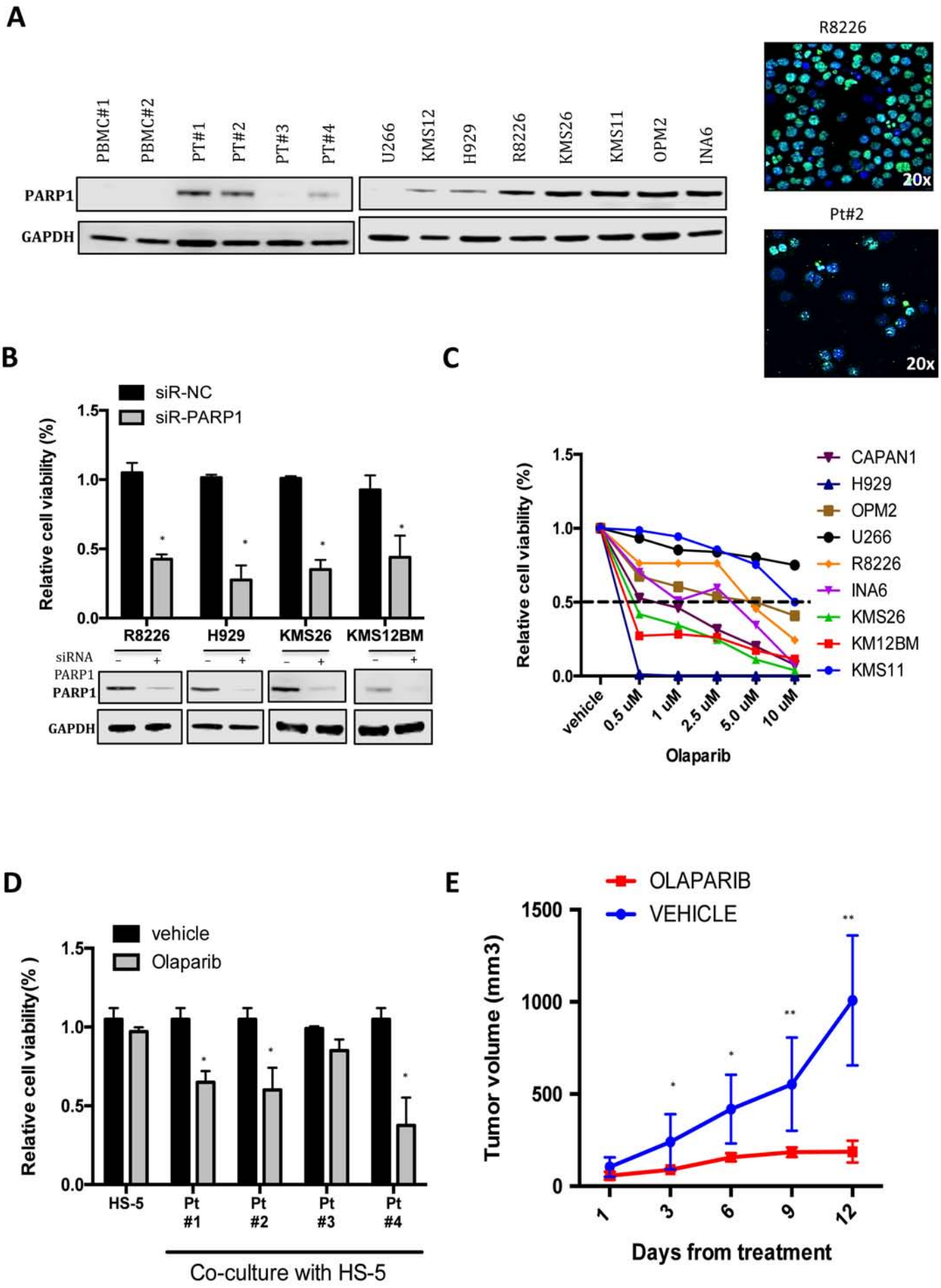
A
PBMC#1
PBMC#2
PT#1
PT#2
PT#3
PT#4
U266
KMS12
H929
R8226
KMS26
KMS11
OPM2
INA6
PARP1
GAPDH
R8226
20x
Pt#2
20x
B
siR-NC
siR-PARP1
Relative cell viability (%)
1.5
1.0
0.5
0.0
R8226
H929
KMS26
KMS12BM
siRNA
PARP1
PARP1
GAPDH
C
Relative cell viability (%)
CAPAN1
H929
OPM2
U266
R8226
INA6
KMS26
KM12BM
KMS11
vehicle
0.5 uM
1 uM
2.5 uM
5.0 uM
10 uM
Olaparib
D
vehicle
Olaparib
Relative cell viability(%)
HS-5
Pt #1
Pt #2
Pt #3
Pt #4
Co-culture with HS-5
E
OLAPARIB
VEHICLE
Tumor volume (mm3)
1500
1000
500
0
1
3
6
9
12
Days from treatment

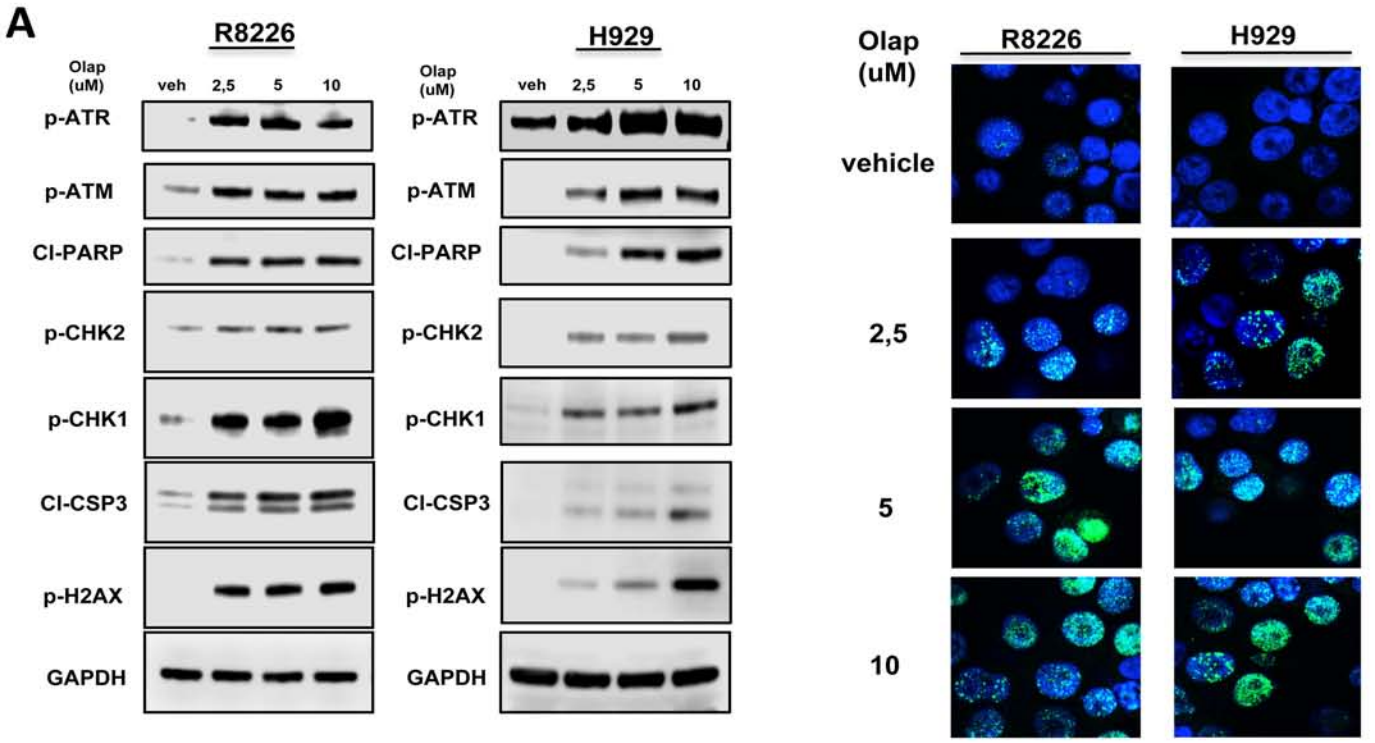
A
R8226
H929
Olap (uM)
veh
2,5
5
10
p-ATR
p-ATM
Cl-PARP
p-CHK2
p-CHK1
Cl-CSP3
p-H2AX
GAPDH
Olap (uM)
R8226
H929
vehicle
2,5
5
10

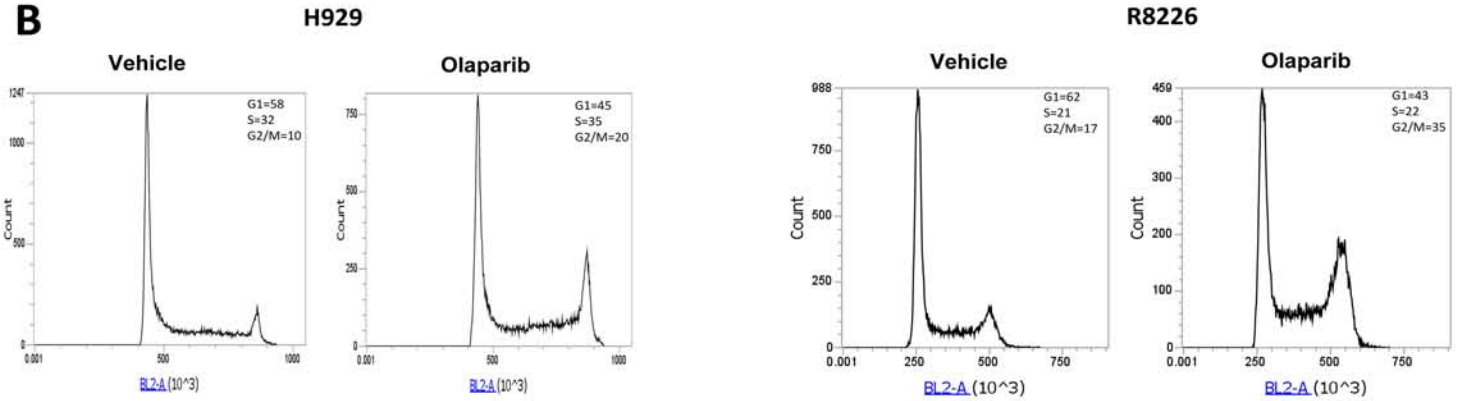
B
H929
Vehicle
Olaparib
G1=58
S=32
G2/M=10
G1=45
S=35
G2/M=20
Count
BL2-A (10^3)
R8226
Vehicle
Olaparib
G1=62
S=21
G2/M=17
G1=43
S=22
G2/M=35
Count
BL2-A (10^3)

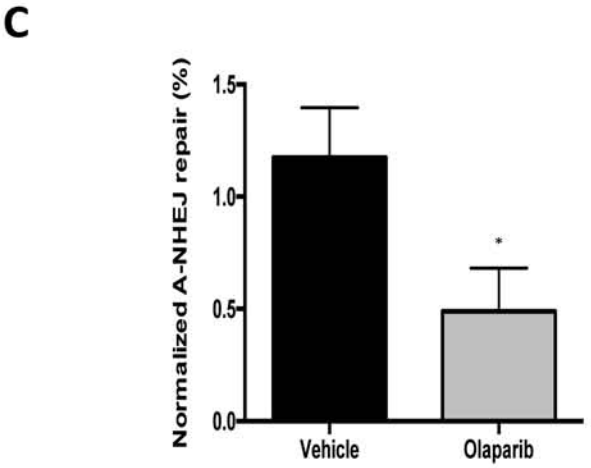
C
Normalized A-NHEJ repair (%)
1.5
1.0
0.5
0.0
*
Vehicle
Olaparib

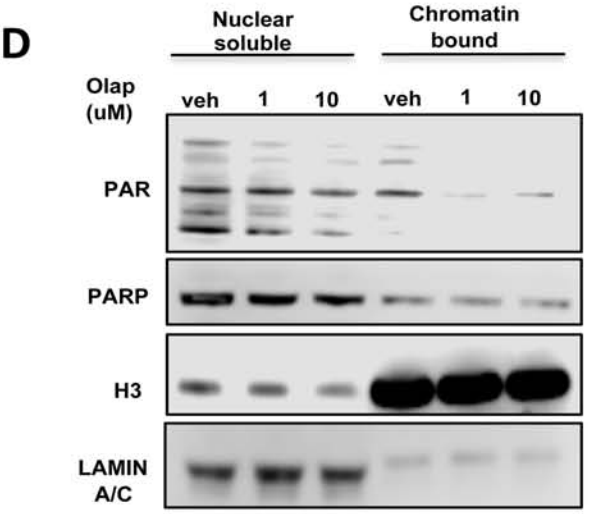
D
Nuclear soluble
Chromatin bound
Olap (uM)
veh
1
10
veh
1
10
PAR
PARP
H3
LAMIN A/C

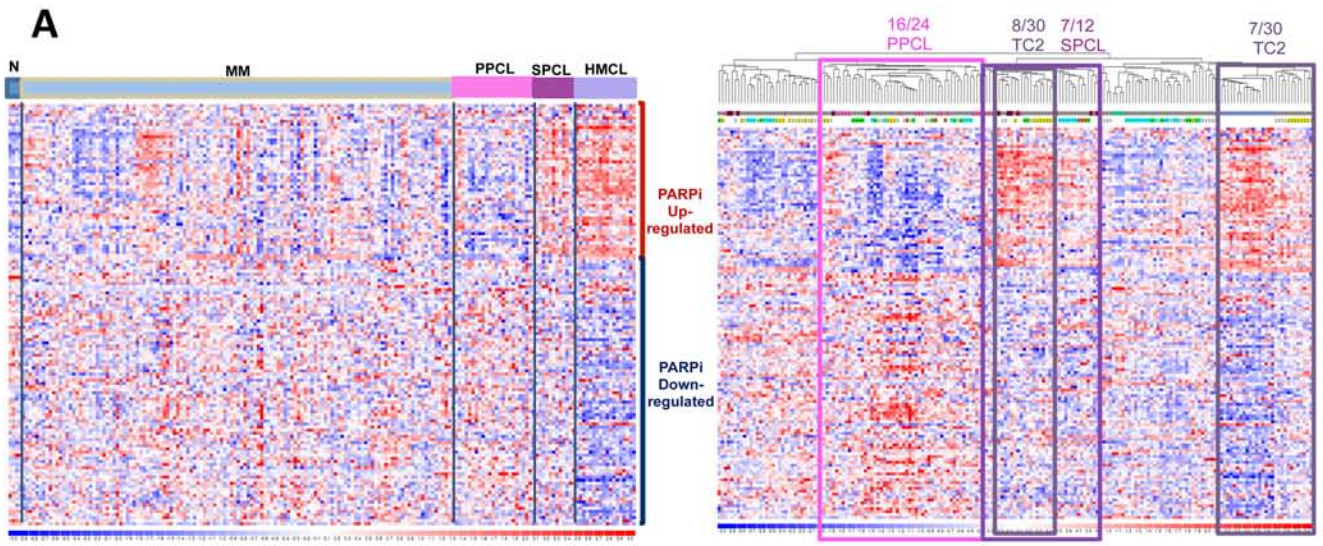
A
N
MM
PPCL
SPCL
HMCL
PARPi Up-regulated
PARPi Down-regulated
16/24 PPCL
8/30 TC2
7/12 SPCL
7/30 TC2

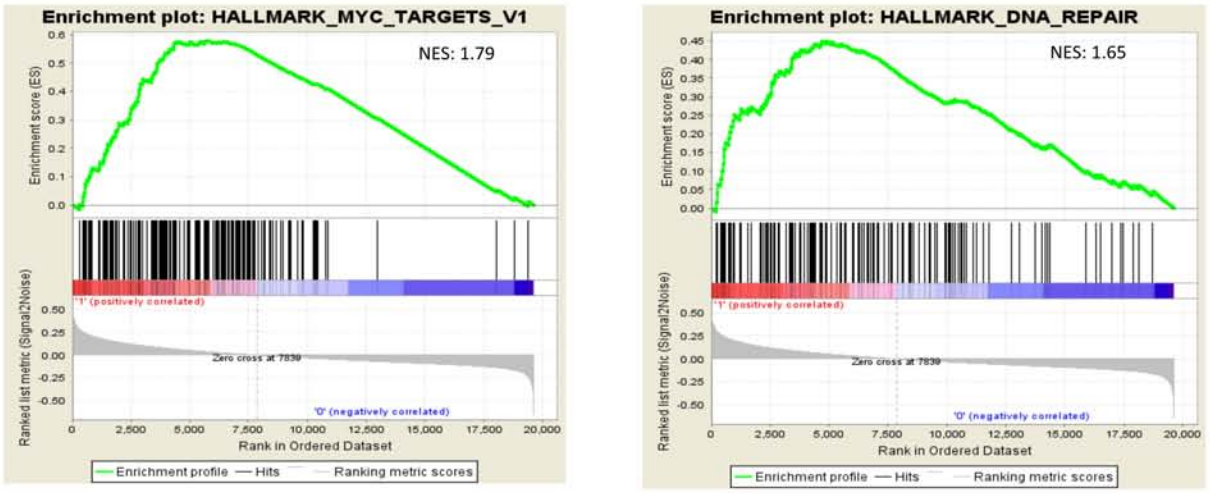
B
Enrichment plot: HALLMARK_MYC_TARGETS_V1
NES: 1.79
Enrichment score (ES)
Ranked list metric (Signal2Noise)
'1' (positively correlated)
Zero cross at 7839
'0' (negatively correlated)
Rank in Ordered Dataset
Enrichment profile
Hits
Ranking metric scores
Enrichment plot: HALLMARK_DNA_REPAIR
NES: 1.65

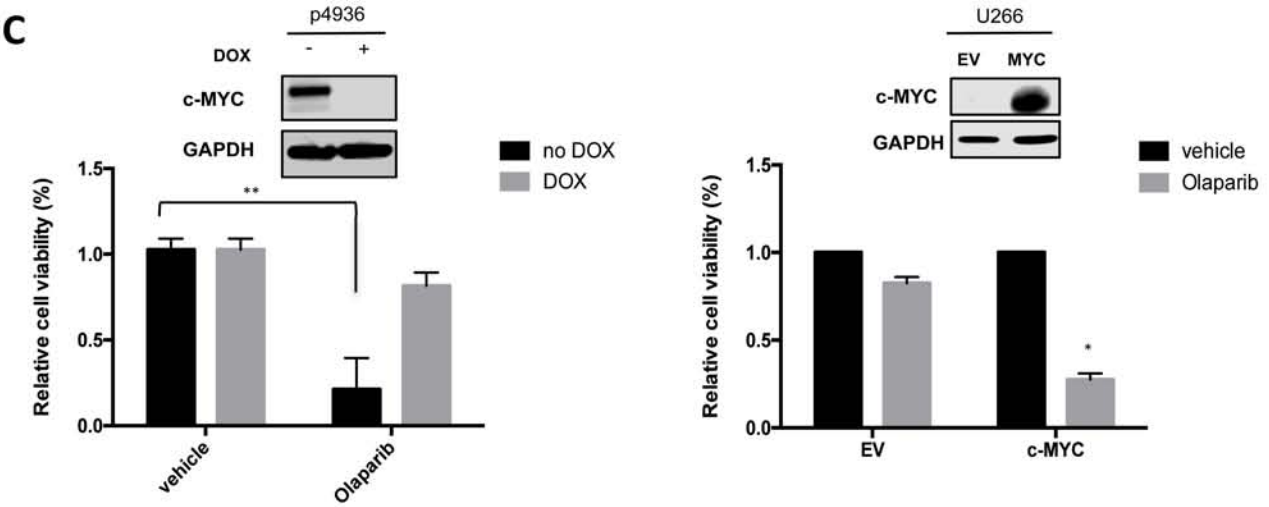
C
p4936
DOX
-
+
c-MYC
GAPDH
no DOX
DOX
Relative cell viability (%)
**
vehicle
Olaparib
U266
EV
MYC
c-MYC
GAPDH
vehicle
Olaparib
Relative cell viability (%)
*
EV
c-MYC

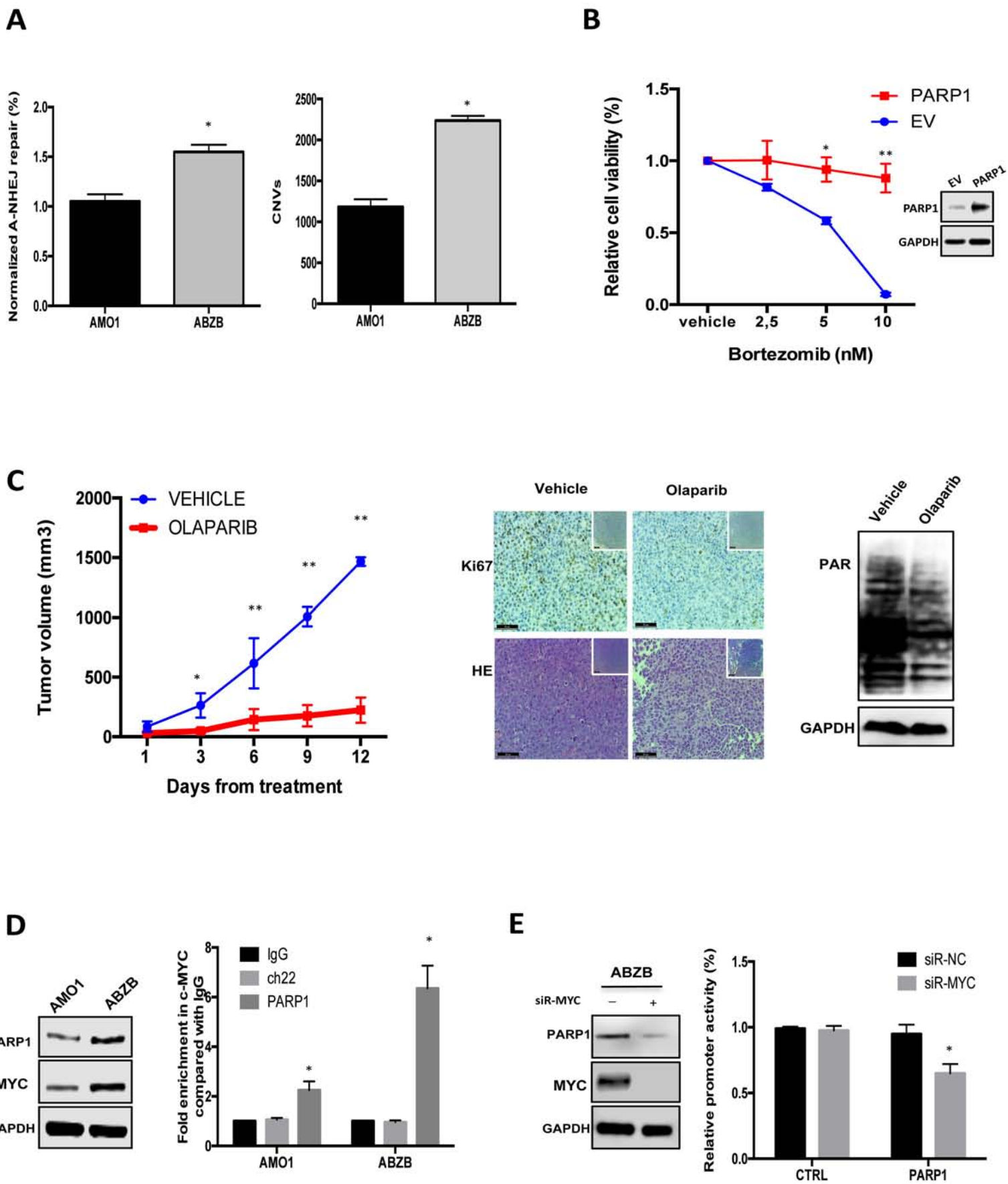
A
Normalized A-NHEJ repair (%)
2.0
1.5
1.0
0.5
0.0
*
AMO1
ABZB
CNVs
2500
2000
1500
1000
500
0
*
AMO1
ABZB
B
Relative cell viability (%)
1.5
1.0
0.5
0.0
PARP1
EV
*
**
vehicle
2,5
5
10
Bortezomib (nM)
EV
PARP1
PARP1
GAPDH
C
Tumor volume (mm3)
2000
1500
1000
500
0
VEHICLE
OLAPARIB
*
**
**
**
1
3
6
9
12
Days from treatment
Vehicle
Olaparib
Ki67
HE
Vehicle
Olaparib
PAR
GAPDH
D
AMO1
ABZB
PARP1
MYC
GAPDH
Fold enrichment in c-MYC compared with IgG
8
6
4
2
0
IgG
ch22
PARP1
*
*
AMO1
ABZB
E
ABZB
siR-MYC
–
+
PARP1
MYC
GAPDH
Relative promoter activity (%)
1.5
1.0
0.5
0.0
siR-NC
siR-MYC
*
CTRL
PARP1

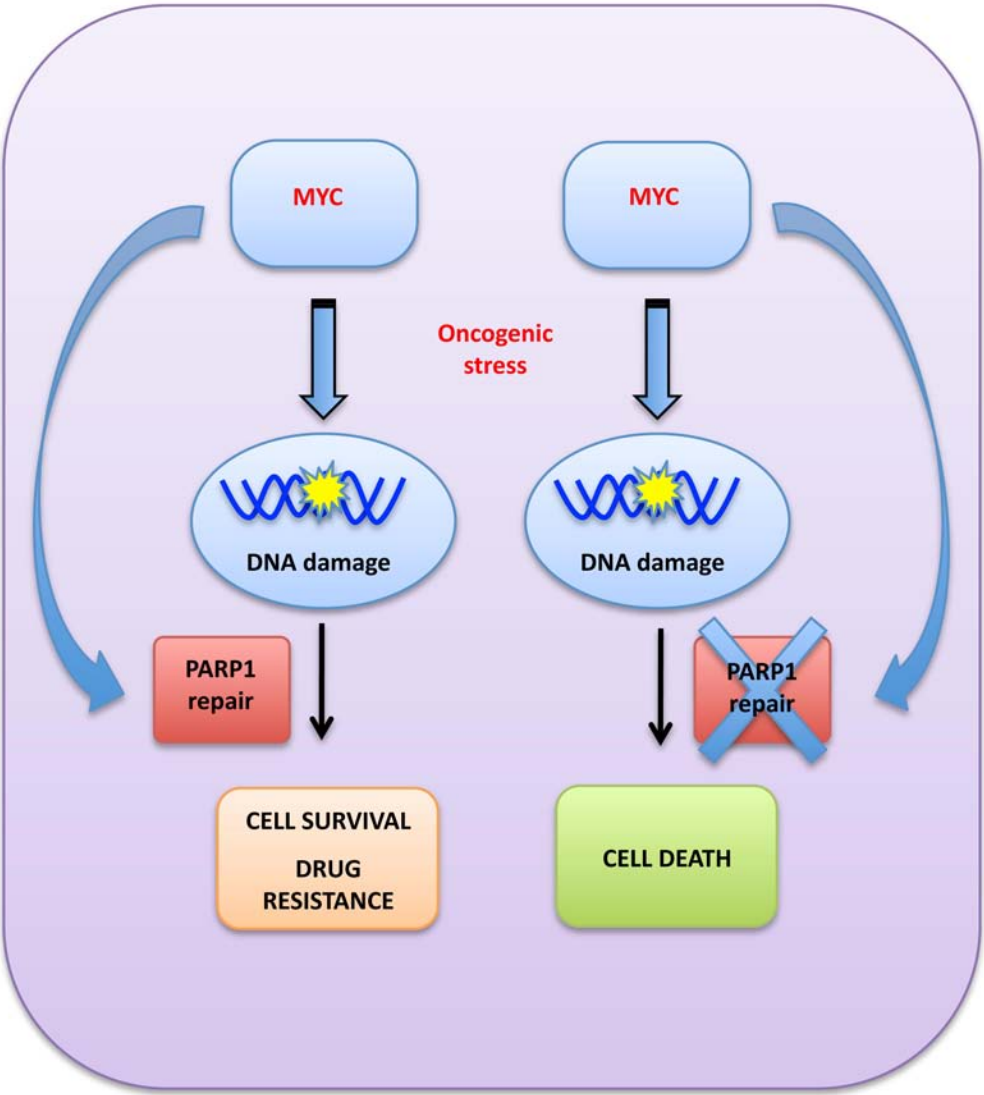
MYC
MYC
Oncogenic stress
DNA damage
DNA damage
PARP1 repair
PARP1 repair
CELL SURVIVAL
DRUG RESISTANCE
CELL DEATH

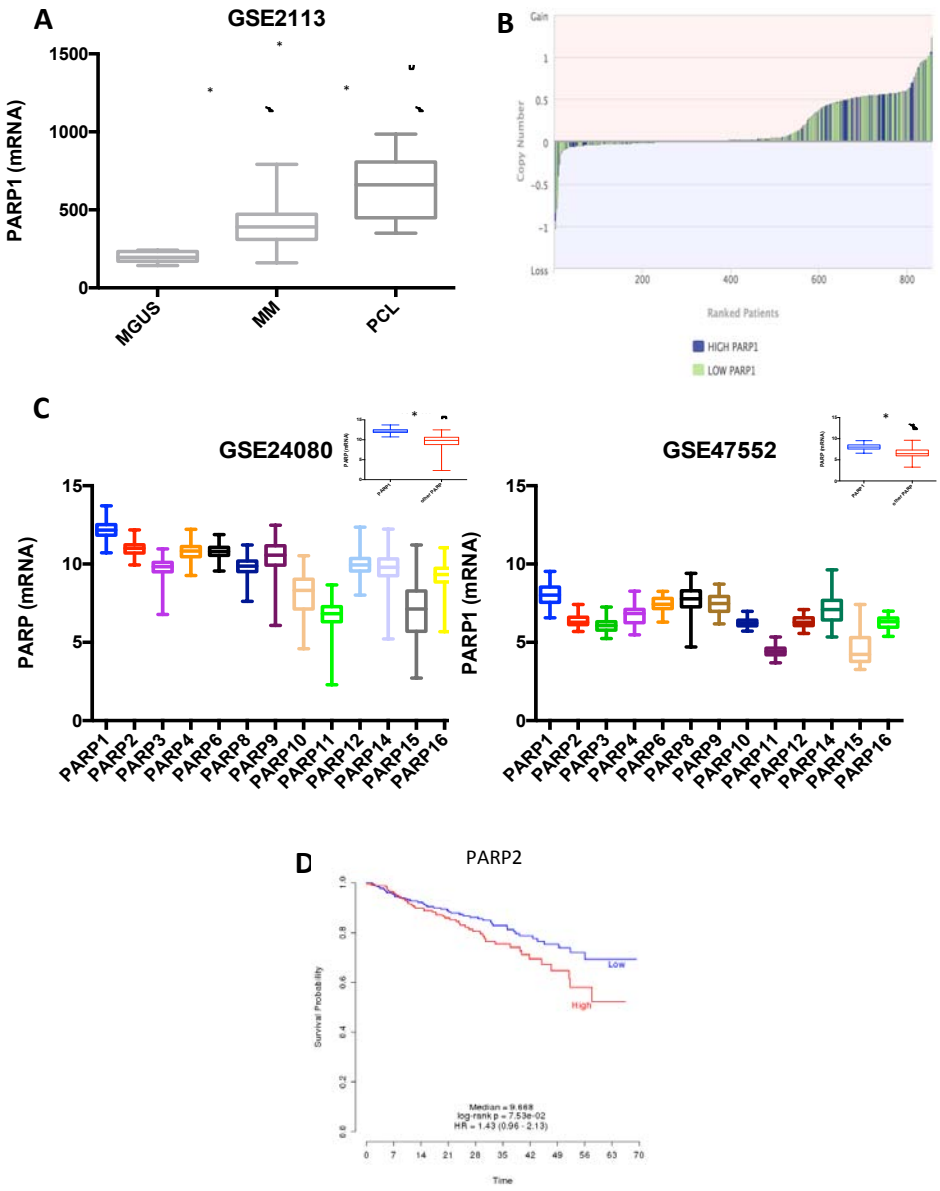

Supplementary Fig.1: (A) Analysis of GSE2113 dataset. PARP1 mRNA levels in MGUS, MM and PCL patients. *, P<0.001 **(B)** Copy number variation analysis of PARP1 gene in MM patients from MMRF researcher gateway portal (https://research.themmrf.org).
(C) Data obtained from GSE24080 and GSE47552 datasets showing PARP family members mRNA expression. **(D)** Data obtained interrogating GSE24080 dataset. Prognostic relevance of PARP2 on Overall Survival (OS)

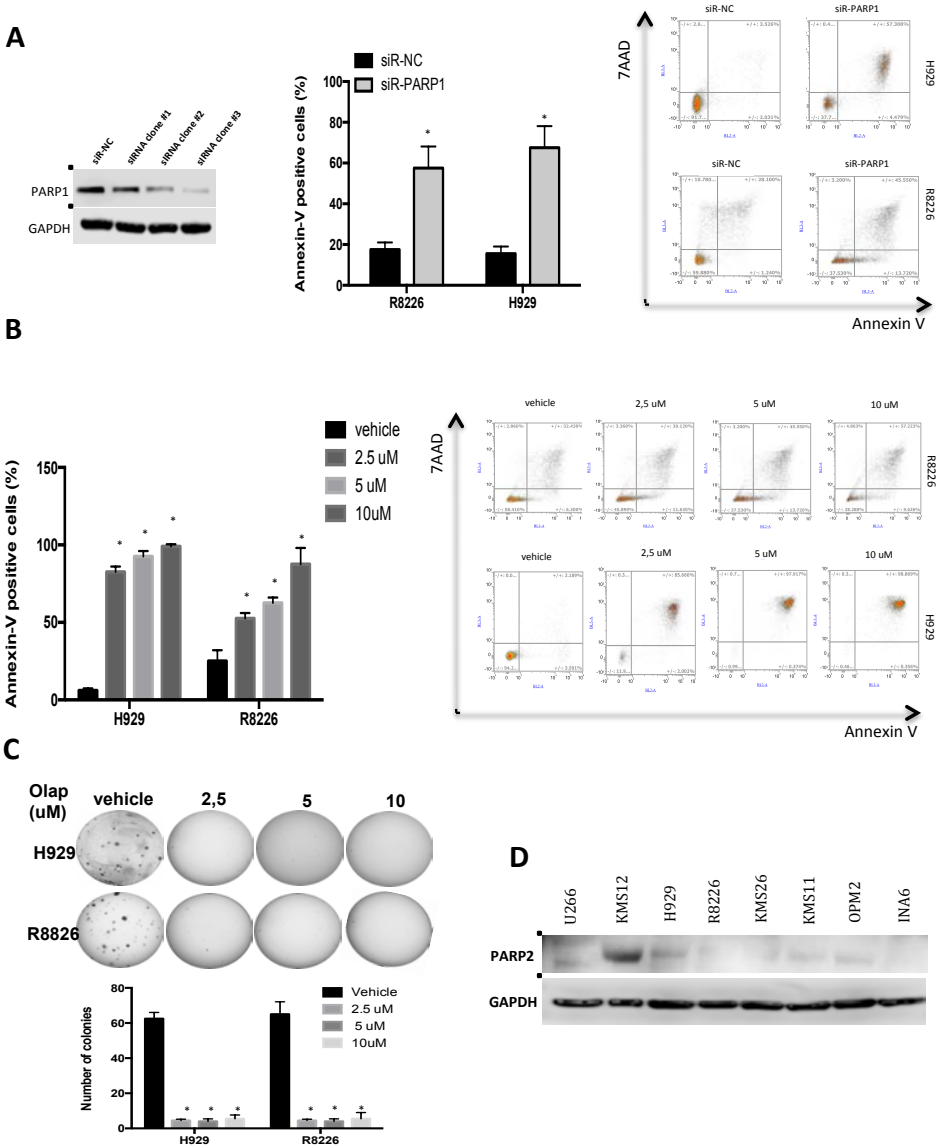

Supplementary Fig.2: (A) *Left:* H929 cells were transfected with scramble control or 3 different PARP1-siRNAs. Immunoblot for PARP1 was performed 48h after transfection. *Right*: Annexin V-positive H929 and R8226 cells 48h transfected with siRNA-NC or PARP1-sIRNA clone #3. **(B)** Indicated MM cells were treated with increasing dose of Olaparib. Annexin V-positive cells 4 days from treatment are shown. **(C)** Colony formation of MM cells treated with vehicle or increasing dose of Olaparib. Light microscopy is shown. Numbers of colonies after 2 weeks (average of 3 independent experiments; *P<0.01) **(D)** Immunoblot analysis of PARP2 levels in MM cell lines

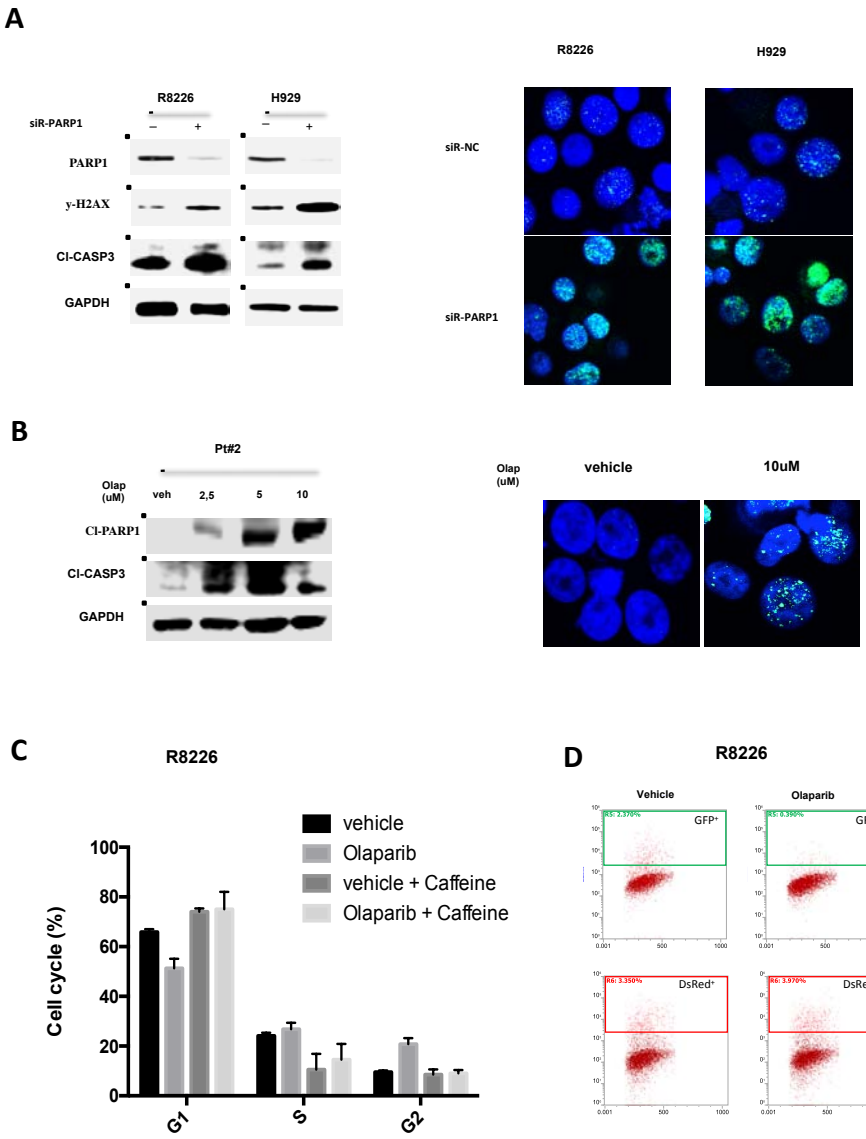

Supplementary Fig.3. (A) *Left*: Immunoblot analysis of PARP1, Cl-Caspase 3 and y-H2AX. GAPDH was used as a loading control. Analysis was performed 48h after transfection. *Right:* γ-H2AX foci evaluation by immunofluorescence 48h after cell transfection. DAPI (blue) was used for nuclear staining. **(B)** Primary MM cells (Pt#2) were treated with increasing dose of Olaparib. *Left*: Immunoblot analysis of PARP1 and Cl-Caspase 3. GAPDH was used as a loading control. Analysis was performed 24h after treatment. *Right:* γ-H2AX foci evaluation by immunofluorescence 24h after treatment. DAPI (blue) was used for nuclear staining. **(C)** R8226 cells were treated with Olaparib in presence or absence of Caffeine (4mM). Cell cycle analysis was performed 24h after treatment. **(D)** FACS traces of Alt-NHEJ repair assay performed on R8226 cells 48h after Olaparib (2,5 uM) treatment. Data are representative of at least three independent experiments

A

MM TC2

NAME	SIZE	NES	NOM p-val	FDR q-val
HALLMARK_MYC_TARGETS_V1	193	1,7856873	0,014373717	0,03468112
HALLMARK_DNA_REPAIR	142	1,6550231	0,017716536	0,058839813
HALLMARK_PROTEIN_SECRETION	95	1,6840036	0,01446281	0,06626201
HALLMARK_E2F_TARGETS	197	1,6056912	0,013861386	0,07338895
HALLMARK_MYC_TARGETS_V2	58	1,5217887	0,0945674	0,09294832
HALLMARK_G2M_CHECKPOINT	198	1,5295784	0,05162524	0,10125281
HALLMARK_OXIDATIVE_PHOSPHORYLATION	199	1,5424293	0,077731095	0,107795745
HALLMARK_UNFOLDED_PROTEIN_RESPONSE	110	1,4343021	0,08151093	0,15497208
HALLMARK_GLYCOLYSIS	197	1,4071164	0,025440313	0,16444612
HALLMARK_FATTY_ACID_METABOLISM	156	1,3859935	0,0977131	0,1699437
HALLMARK_MITOTIC_SPINDLE	198	1,3431541	0,1375969	0,2012267
HALLMARK_KRAS_SIGNALING_DN	191	-1,5732522	0,00203666	0,24661924

PCL

NAME	SIZE	NES	NOM p-val	FDR q-val
HALLMARK_PROTEIN_SECRETION	95	1,7689918	0,006012024	0,01914201
HALLMARK_MYC_TARGETS_V1	193	1,667538	0,023904383	0,05121669
HALLMARK_MTORC1_SIGNALING	195	1,556562	0,031746034	0,08666427
HALLMARK_OXIDATIVE_PHOSPHORYLATION	199	1,5660286	0,07456979	0,10556252
HALLMARK_MYC_TARGETS_V2	58	1,3731388	0,17254902	0,12093651
HALLMARK_MITOTIC_SPINDLE	198	1,4240882	0,04752066	0,12270054
HALLMARK_REACTIVE_OXIGEN_SPECIES_PATHWAY	47	1,377877	0,08262712	0,1270538
HALLMARK_DNA_REPAIR	142	1,4478067	0,09001957	0,13369577
HALLMARK_E2F_TARGETS	197	1,427879	0,09306931	0,13458158
HALLMARK_G2M_CHECKPOINT	198	1,3809469	0,14395393	0,13568851
HALLMARK_PEROXISOME	102	1,487821	0,010204081	0,13685687
HALLMARK_FATTY_ACID_METABOLISM	156	1,4614549	0,057026476	0,14129122
HALLMARK_ADIPOGENESIS	**195**	**1,3854795**	**0,06378601**	**0,14467503**
HALLMARK_GLYCOLYSIS	197	1,2754492	0,1663286	0,20073012
HALLMARK_KRAS_SIGNALING_DN	191	-1,6577327	0	0,13666743

B

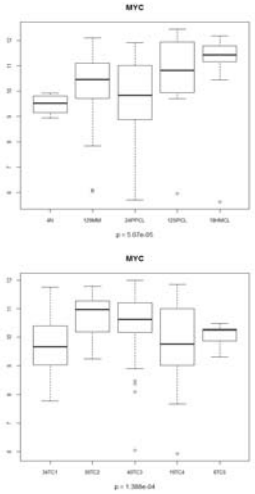

C

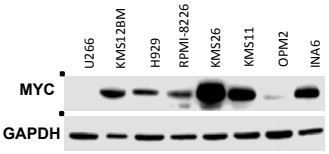

D

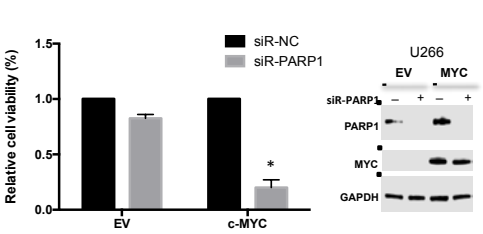

E

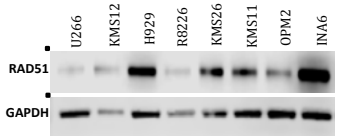

	1q WT	1q gain	TOT	Two-tailed P value equals 1.0000
PARPI-NEG	9	10	19	
PARPI-POS	4	6	10	
TOT	13	16	29	
	13q WT	**del(13q)**	**TOT**	The two-tailed P value equals 1.0000
PARPI-NEG	11	3	14	
PARPI-POS	13	3	16	
TOT	24	6	30	
	NHD	**HD**	**TOT**	The two-tailed P value equals 1.0000
PARPI-NEG	3	10	13	
PARPI-POS	4	11	14	
TOT	7	21	27	
	DIS3 WT	**DIS3 mut**	**TOT**	The two-tailed P value equals 0.2262
PARPI-NEG	13	0	13	
PARPI-POS	12	3	15	
TOT	25	3	28	
	BRAF WT	**BRAF mut**	**TOT**	The two-tailed P value equals 0.5956
PARPI-NEG	11	2	13	
PARPI-POS	13	2	15	
TOT	24	4	28	
	NRAS WT	**NRAS mut**	**TOT**	The two-tailed P value equals 1.0000
PARPI-NEG	8	5	13	
PARPI-POS	9	6	15	
TOT	17	11	28	
	KRAS WT	**KRAS mut**	**TOT**	The two-tailed P value equals 1.0000
PARPI-NEG	8	5	13	
PARPI-POS	9	6	15	
TOT	17	11	28	

Supplementary Fig.4: (A) List of significant gene sets (nominal p-value <0.05) from GSEA analysis, using Hallmark collection in MM-TC2 and PCL PARPi-positive versus PARPi-negative comparison. Normalized Enrichment Score (NES), Nominal p-value and FDR q-value are reported for each significant gene set. **(B)** Box plots of *MYC* gene expression profiles (log scale) in PC dyscrasias' dataset and e) in 129 MM samples stratified according to five TC classes. P-value by Kruskal-Wallis test is reported. **(C)** Immunoblot analysis of MYC protein levels in MM cell lines. GAPDH, used as a loading control, is the same shown in Fig-2A. **(D)** U266 EV or MYC$^+$ were transfected with scramble control or PARP1-siRNA. *Right panel*: Immunoblot analysis of PARP1. GAPDH was used as a loading control. Analysis was performed 48h after transfection. *Left panel*: CTG assay was performed on 4 days after transfection. **(E)** *Left panel:* Immunoblot analysis of RAD51 levels in MM cell lines. *Right panel:* Fisher's exact test on TC2-MM cases stratified according to main molecular alterations evaluated by FISH (cytogenetic abnormalities) and NGS (somatic mutations)

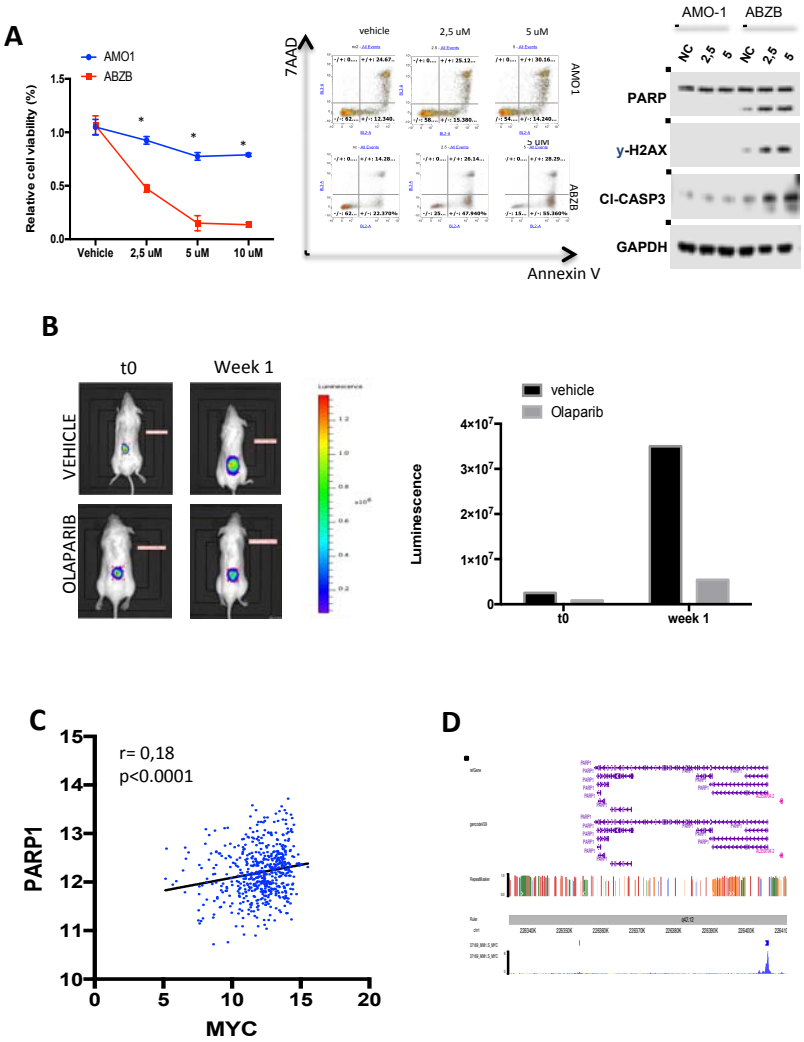

Supplementary Fig.5 (A) *Left panel*: Cell viability of AMO1 and ABZB, treated with vehicle or Olaparib for 7 days. *Middle panel*: Annexin V positive AMO1 and ABZB cells, treated with vehicle or Olaparib for 4 days. . *Right panel:* Immunoblot of PARP1, Cl-Caspase 3 and y-H2AX. GAPDH was used as a loading control. Analysis was performed 24h after treatment. **(B)** Representative IVIS images and BLI-based measurement of tumor volumes (5 animals for each group) of NOD SCID mice s.c. xenografted with luciferase gene-marked ABZB, were performed before (t0) and 1 week after treatment. **(C)** Graphs of correlations between endogenous mRNA expression levels of PARP1 and MYC in MM patients from GSE24080 dataset. **(D)** Graphical results of bio-informatic screening (cistrome.org) showing c-MYC binding consensus sequences to PARP1 promoter.
Data are representative of at least three independent experiments. *P<0.05.

Supplementary Material and Methods

Multiple myeloma cell lines, primary cells, and reagents

Peripheral blood mononuclear cells (PBMCs) and primary cells from multiple myeloma patient bone marrow aspirates, following informed consent and University Magna Graecia (Catanzaro, Italy) IRB approval, were isolated using Ficoll–Hypaque density gradient sedimentation as reported previously (1). Multiple myeloma patients' cells were separated from bone marrow samples by antibody-mediated selection using anti-CD138 magnetic-activated cell separation microbeads (Miltenyi Biotec). Purity of immunoselected cells was assessed by flow-cytometry analysis using a phycoerythrin-conjugated CD138 monoclonal antibody by standard procedures. CD138+ cells from MM patients pt#1, pt#2 and pt#3 were cultured in RPMI-1640 medium (Gibco®, Life Technologies) supplemented with 20% fetal bovine serum (Lonza Group Ltd.) and 1% penicillin/streptomycin (Gibco®, Life Technologies). Multiple myeloma cell lines (HMCLs) AMO1, NCI-H929, U266, KMS12-BM were purchased from DSMZ (Braunschweig, Germany). CAPAN1, RPMI-8226 and OPM2 were purchased from ATCC (Manassas, VA, USA). KMS-11 were kindly provided by Dr. K.C. Anderson (Dana-Farber Cancer Institute, Harvard Medical School, Boston, MA, USA). KMS-26 were kindly provided by Dr. Giovanni Tonon (University of San Raffaele Scientific Institute, Milan, Italy). P493-6 were kindly provided by Dr.Dirk Eick (Max Planck Institute of Biochemistry, Helmholtz-Zentrum München, Germany and cultured in RPMI-1640 medium (Gibco® Life Technologies) supplemented with 10% fetal bovine serum (Lonza Group Ltd.) and 1% penicillin/streptomycin (Gibco®, Life Technologies). AMO1 bortezomib-resistant (ABZB) were kindly provided by Dr. Christoph Driessen (Eberhand Karls University, Tübingen, Germany). Multiple myeloma cell lines were cultured in RPMI1640 (Gibco, Life Technologies) supplemented with 10% FBS (Lonza Group). INA-6 cell line (kindly provided by Dr. Renate Burger, University of Erlangen- Nuernberg, Germany) was cultured in the presence of recombinant human IL6 (2,5 ng/mL, R&D Systems, Minneapolis, MN); this cell line was not further authenticated but confirmed for the described IL6 dependence. HS-5 human stromal cell line (purchased from ATCC, CRL-11882TM) was cultured in DMEM supplemented with 10% fetal bovine serum and 1% penicillin/streptomycin . Co-culture experiments were performed in 6 well plate at a density of 2,5 × 10 5 cells/ ml in 1:1 HS-5 /MM cells ratio. All these cell lines were immediately frozen and used from the original stock within 6 months.

Transduction of cells

To generate cells stably expressing luciferase transgene, ABZB cells were transduced with pLenti-III-PGK-Luc (ABM Inc., Richmond, BC, Canada) vector, the manufacturer's instructions. To generate cells stably expressing c-MYC, U266 were transduced with Precision LentiORF human MYC (GE Dharmacon, Lafayette, Colorado, USA).

Gene expression profiling

PARPi signature was evaluated in a PC dyscrasias dataset, including samples from 129 MM, 24 primary PCL (PPCL) at onset and 12 secondary PCL (SPCL) cases, together with 18 HMCL and 4 healthy donors (N) samples, that were profiled on Affymetrix Gene 1.0 ST array (GSE66293)(2). MM samples were stratified according to TC classification (3) in 34 TC1, 30 TC2, 40 TC3, 19 TC4 and 6 TC5, respectively.

Global gene expression profiles were extracted for almost the entire PARPi gene list (27/28, 96% up-regulated and 111/119, 93% down-regulated genes). Hierarchical agglomerative clustering (Pearson's correlation and average linkage methods) was applied to identify sub-groups of samples with similar gene expression patterns.

A Gene Set Enrichment Analysis (GSEA) (4) was applied on global gene expression profiles of 16 MM-TC2 samples showing PARPi-positive versus 14 MM-TC2 cases carrying PARPi-negative expression patterns, grouped on the base of clustering analysis. Similarly, 13 PARPi-positive versus 23 PARPi-negative PCL samples were compared by GSEA analysis. Phenotype permutations and default analysis's conditions were applied on Hallmark gene set collection and significant gene sets were selected based on FDR q-value < 25%.

Differential expression analysis of MYC gene expression levels across PC dyscrasias and MM TC classes was performed by means of Kruskal-Wallis test, by using *stat* package in R software. Dunn's test was used for multiple pairwise comparisons and the Benjamini and Hochberg correction was applied to adjust significance of multiple tests (adjusted $p < 0.05$).

In vitro transfection of MM cells

Stealth™ PARP1 siRNA (clone IDs: HSS100243, HSS100244, HSS100245) and Silencer TM select MYC (clone IDs: s9129) were purchased from Invitrogen™ (Thermo Scientific). All the oligos were used at 100 nmol/L final concentration. MM cells were transfected using Neon Transfection System (Invitrogen™) (2 pulse at 1.050 V, 30 milliseconds). The same conditions were applied for transfection of MM cells with 2,5 μg of expression vectors carrying the ORFs of PARP1 NM_001618.3 (EX-Z8307-M68), with empty vector (EV) used as control (EX-NEG-M68) (GeneCopeia, Rockville, MD, USA).

DSB repair assay

In vivo DSB repair assays were performed as previously described (5, 6). Briefly, EJ2-GFP plasmid (#44025, Addgene) was linearized with I-SceI (Thermo Scientific) digestion and transfected into $1x10^6$ cells at a ratio of 1ug per well. In parallel, cells were transfected using with 0.1 μg of DsRed-N1 plasmid (kindly provided by Dr.Michele Cea, Dana-Farber Cancer Institute, Boston, MA) as the internal control. 48h after Olaparib treatment, the numbers of GFP+ and DsRed+ cells were determined by flow cytometry (Attune NxT, Thermo Fisher Scientific). For each experiment, FACS analyzed a minimum of 20,000 cells. The ratio between GFP+ and DsRed+ cells was used as a measure Alt-NHEJ repair efficiency.

ChIP

Cells (1.5 x107) were crosslinked in 1% formaldehyde, lysed and sheared by sonication for

10 cycles (each of 30 seconds) on a cold block with 90 seconds time intervals of cooling using the Bioruptor Plus (Diagenode). Chromatin was divided into equal amounts of immunoprecipitation with the MYC antibody (ab56), or rabbit IgG as negative control (Santa Cruz Biotechnology). Chromatin extracts were incubated on a rotator with 20 ml of ChIP Grade Protein A/G Plus Agarose for 3 h at 4°C. Bound agarose beads were harvested by centrifugation (12.000 rpm, 15 seconds) and washed; the precipitated protein-DNA complexes were eluted from washed beads and incubated twice at 65°C for 1.5 h with NaCl and Proteinase K to revert cross-links.

Purified DNA was subjected to qPCR using GoTaq qPCR Master Mix (Promega). Primer sequences for qPCR were:

PARP1(forward) 5′-GGTCTCAAACTCCTGCTACAA-3′

PARP1(reverse) 5'-AGGACACACTTAAGAGTTTGGG-3'

Ch22(forward) 5'- GGATGACAGGCATGAGGAATTA-3'

Ch22(reverse) 5'- TGCTGCTTACTTGGGATATGAG-3'

Promoter activity assay

ABZB cells were co-transfected with siRNA control or MYC–targeting siRNA and negative control (NEG-PG04) or PARP1 (HPRM43771-PG04) promoter constructs (GeneCopeia, Rockville, MD, USA). Measurement of promoter activity was performed with Secrete-Pair ™ Dual Luminescence Assay Kit (GeneCopeia, Rockville, MD, USA) according to manufacturers's instructions

SNP-array data analysis

DNA was extracted from the AMO1 and ABZB cells using the Perfect Pure DNA Blood kit (5 Prime) and analyzed using the Affymetrix Cytoscan HD array (Affymetrix, Inc., Santa Clara, CA) according to manufacturers's instructions, to estimate genomic instability and ongoing DNA rearrangements. This array consists of 2.67 million markers for copy number variation (CNV) analysis, including 750,000 SNP and 1.9 million non- polymorphic probes, with an average spacing for RefSeq genes of 880 bp. Analysis of intensity data (CEL file) was performed with Chromosome Analysis Suite v 3.1 (ChAS 3.1) software using the Affymetrix HapMap Reference Model File for comparison. We used 25 probes and > 25 kb and >50 kb as a minimum cutoff for deletions and gains respectively. Map position was based on GRCh37/hg19 assembly.

Histology and immunohistochemistry

Retrieved tumors from animals were fixed in 4% buffered formaldehyde and 24 hours later washed, dehydrated, and embedded in paraffin. For light microscopy analysis by an optical microscope Nikon i55 (Nikon Corporation, Tokyo, Japan), we performed staining with H&E on 4-mm tumor sections mounted on poly-lysine slides. For IHC staining, 2-mm–thick tumor slices were de-paraffinized and pretreated with the Epitope Retrieval Solution 2 (EDTA buffer, pH 8.8) at 98 C for 20 minutes. After washing steps, peroxidase blocking was carried out for 10 minutes using the Bond Polymer. All procedures were performed using the Bond Max Automated Immunohistochemistry. Tissues were washed and incubated with the primary antibody directed against Ki-67 (Dako, clone MIB-1; 1:150). Subsequently, tissues were incubated with

polymer for 10 minutes and developed with DAB–Chromogen for 10 minutes. Slides were counterstained with Hematoxylin.

List of Antibodies

Antibodies	**Sources**	**Catalog #**	**Applications**
Cleaved-Caspase 3 (Asp175)	Cell Signaling Technology	9661	WB (1:1000)
GAPDH	Santa Cruz	25778	WB (1:1000)
PARP	Cell Signaling Technology	9532	WB (1:1000)
Phospho-CHK1 (Ser345)	Cell Signaling Technology	2348	WB (1:1000)
phospho-CHK2 (Thr 68)	Cell Signaling Technology	2197	WB (1:1000)
phospho-ATM (Ser 1981)	Cell Signaling Technology	5883	WB (1:1000)
phospho-ATR (Ser 428)	Cell Signaling Technology	2853	WB (1:1000)
phospho-Histone H2A.X (Ser139)	Cell Signaling Technology	9718	WB (1:1000) IF (1:200) IHC (1:480)

c-Myc	Cell Signaling Technology	5605	WB (1:1000)
PARP2	Santa Cruz	393343	WB (1:1000)
RAD51	Cell Signaling Technology	8875	WB (1:1000)
Goat anti-rabbit IgG-HRP	Santa Cruz	2054	WB (1:3000)
Goat anti-mouse IgG-HRP	Santa Cruz	2055	WB (1:3000)

WB, western blot. ChIP, chromatin immunoprecipitaion. IF, immunofluorescence. IHC,

immunohistochemistry

References

1. Amodio N, Di Martino MT, Foresta U, Leone E, Lionetti M, Leotta M, et al. miR-29b sensitizes multiple myeloma cells to bortezomib-induced apoptosis through the activation of a feedback loop with the transcription factor Sp1. Cell death & disease. 2012;3:e436.
2. Lionetti M, Barbieri M, Todoerti K, Agnelli L, Marzorati S, Fabris S, et al. Molecular spectrum of BRAF, NRAS and KRAS gene mutations in plasma cell dyscrasias: implication for MEK-ERK pathway activation. Oncotarget. 2015;6(27):24205-17.
3. Hideshima T, Bergsagel PL, Kuehl WM, Anderson KC. Advances in biology of multiple myeloma: clinical applications. Blood. 2004;104(3):607-18.
4. Subramanian A, Tamayo P, Mootha VK, Mukherjee S, Ebert BL, Gillette MA, et al. Gene set enrichment analysis: a knowledge-based approach for interpreting genome-wide expression profiles. Proceedings of the National Academy of Sciences of the United States of America. 2005;102(43):15545-50.
5. Bennardo N, Cheng A, Huang N, Stark JM. Alternative-NHEJ is a mechanistically distinct pathway of mammalian chromosome break repair. PLoS genetics. 2008;4(6):e1000110.
6. Czochor JR, Sulkowski P, Glazer PM. miR-155 Overexpression Promotes Genomic Instability by Reducing High-fidelity Polymerase Delta Expression and Activating Error-Prone DSB Repair. Molecular cancer research : MCR. 2016;14(4):363-73.